




Article

Anhydrous alkali copper sulfates – a promising playground for new Cu^{2+} oxide complexes: new Rb-analogues of fumarolic minerals.

Oleg I. Siidra^{1,2*} , Diana O. Nekrasova^{1,3}, Dmitry O. Charkin⁴, Anatoly N. Zaitsev⁵, Artem S. Borisov¹, Marie Colmont³, Olivier Mentré³ and Darya V. Spiridonova¹

¹Department of Crystallography, St. Petersburg State University, University Embankment 7/9, 199034 St. Petersburg, Russia; ²Kola Science Center, Russian Academy of Sciences, Apatity, 184200, Murmansk Region, Russia; ³Université Lille, CNRS, Centrale Lille, Université Artois, UMR 8181, Unité de Catalyse et Chimie du Solide, Lille, F-59000, France; ⁴Department of Chemistry, Moscow State University, GSP-1, Moscow 119991, Russia; and ⁵Department of Mineralogy, St. Petersburg State University, University Embankment 7/9, 199034 St. Petersburg, Russia

Abstract

We report the crystal structures of eight new synthetic multinary Rb–Cu sulfates representing four new structure types: $\delta\text{-Rb}_2\text{Cu}(\text{SO}_4)_2$, $\gamma\text{-RbNaCu}(\text{SO}_4)_2$, $\gamma\text{-RbKCu}(\text{SO}_4)_2$, $\text{Rb}_2\text{Cu}_2(\text{SO}_4)_3$, $\text{Rb}_2\text{Cu}_2(\text{SO}_4)_3(\text{H}_2\text{O})$, $\beta\text{-Rb}_2\text{Cu}(\text{SO}_4)\text{Cl}_2$, $\beta\text{-Rb}_4\text{Cu}_4\text{O}_2(\text{SO}_4)_4(\text{Cu}_{0.83}\text{Rb}_{0.17}\text{Cl})$ and $\text{Rb}_2\text{Cu}_5\text{O}(\text{SO}_4)_5$. The determination of their crystal structures significantly expands the family of anhydrous copper sulfates. Some of the anhydrous rubidium copper sulfates obtained turned out to be isostructural to known compounds and minerals. $\text{Rb}_2\text{Cu}_5\text{O}(\text{SO}_4)_5$ is isostructural to cesiodymite, $\text{CsKCu}_5\text{O}(\text{SO}_4)_5$ and cryptochalcite, $\text{K}_2\text{Cu}_5\text{O}(\text{SO}_4)_5$. $\text{Rb}_2\text{Cu}_2(\text{SO}_4)_3$ also shows an example of crystallisation in the already known structure type first observed for synthetic $\text{K}_2\text{Cu}_2(\text{SO}_4)_3$. ‘Hydrolangbeinite’, $\text{Rb}_2\text{Cu}_2(\text{SO}_4)_3(\text{H}_2\text{O})$, was formed as a result of a minor hydration of the initial mixture of reagents.

The minerals and synthetic framework compounds of the $\text{A}_2\text{Cu}(\text{SO}_4)_2$ series demonstrate a vivid example of morphotropism with the formation of structural types depending on the size of the cations residing in the cavities of the $[\text{Cu}(\text{SO}_4)_2]^{2-}$ open framework. To date, five types (α , β , γ , δ and ϵ) can be distinguished. We propose to call this series of compounds ‘saranchinaite-type’, as the stoichiometry $\text{A}_2\text{Cu}(\text{SO}_4)_2$ was first encountered during the discovery and description of saranchinaite, $\text{Na}_2\text{Cu}(\text{SO}_4)_2$.

The discovery of $\beta\text{-Rb}_2\text{Cu}(\text{SO}_4)\text{Cl}_2$, a new monoclinic polymorph of chlorothionite, seems to be of particular interest considering the recently discovered interesting magnetic properties of synthetic $\text{K}_2\text{Cu}(\text{SO}_4)\text{X}_2$ ($\text{X} = \text{Cl}$ and Br) and $\text{Na}_2\text{Cu}(\text{SO}_4)\text{Cl}_2$.

In these new structural architectures, a number of features have been revealed that were seldom observed previously. The first is the bidentate coordination of the sulfate tetrahedron via edge-sharing with the Cu^{2+} -centred coordination polyhedron. Until recently, such coordination was known only for the chlorothionite structure. The second is formation of ‘high-coordinate’ CuO_7 polyhedra. The structures of the new compounds suggest that such coordination is not in fact so uncommon, at least among anhydrous alkali copper sulfates. All of the described features clearly indicate the importance of further systematic studies of anhydrous copper-sulfate systems. Their exploration, particularly of the new copper-oxide substructures with new coordination environments, is highly likely to lead to new potentially interesting magnetic properties due to the unusual arrangements of magnetically active Cu^{2+} cations.

In addition to experimental details on the synthesis of rubidium analogues of anhydrous potassium and sodium sulfates, this work also provides an analysis and a brief review of the geochemistry of rubidium in volcanic environments.

Keywords: copper, rubidium, sulfates, fumarolic minerals, solid state reactions, gas transport reactions, crystal structures

(Received 11 August 2021; accepted 24 September 2021; Accepted Manuscript published online: 29 September 2021; Associate Editor: Daniel Atencio)

Introduction

A decade ago, the amount of structurally characterised anhydrous sulfates of copper and alkali metals was very limited. Most of the known compounds belonged to minerals from volcanic fumaroles. Euchlorine, $\text{KNaCu}_3\text{O}(\text{SO}_4)_3$ (Scordari and Stasi, 1990; Siidra *et al.*, 2019a), and chlorothionite, $\text{K}_2\text{Cu}(\text{SO}_4)\text{Cl}_2$ (Giacovazzo *et al.* 1976), were discovered more than a century ago in fumaroles of Vesuvius volcano, Italy. Much later, after

the Great Fissure Tolbachik Eruption in Kamchatka in 1975–1976, a large number of new endemic anhydrous copper sulfates were identified (Vergasova and Filatov, 2012). The overwhelming majority of the latter belonged to new structure types and had no known synthetic analogues. A well-known characteristic of transition metal sulfates is their excellent solubility and hydration in air resulting in the appearance of a large number of reaction by-products. The latter requires special conditions during transportation and work in the laboratory. Despite the significant number of articles on copper and alkali metal sulfates that have appeared in the last few years, rubidium copper sulfates are almost unknown. It is known that in the series of alkali metals from Na to Cs in the structures of oxides and oxyalts the phenomenon of morphotropism is observed commonly. As a rule, potassium and

*Author for correspondence: Oleg I. Siidra, Email: o.siidra@spbu.ru

Cite this article: Siidra O.I., Nekrasova D.O., Charkin D.O., Zaitsev A.N., Borisov A.S., Colmont M., Mentré O. and Spiridonova D.V. (2021) Anhydrous alkali copper sulfates – a promising playground for new Cu^{2+} oxide complexes: new Rb-analogues of fumarolic minerals. *Mineralogical Magazine* 85, 831–845. <https://doi.org/10.1180/mgm.2021.73>

rubidium representatives are typically isostructural, whereas sodium and caesium examples can adopt their own structure types.

The wave of interest in anhydrous transition metal sulfates and alkalis in the 2010s is associated with access to specific magnetic cluster-topology (Fujihala *et al.*, 2017, 2018; Furrer *et al.*, 2018), and also with the search for novel electrode materials for possible application as cathodes in rechargeable metal-ion batteries (Masquelier and Croguennec, 2013). For such applications sulfates represent a promising class of compounds given their superior electronegativity and high redox potential by the inductive effect (Rousse and Tarascon, 2014).

In addition to experimental work aimed at the synthesis of rubidium analogues of anhydrous potassium and sodium sulfates, one of the goals of this work was also an analysis and a brief review, below, of the geochemistry of rubidium in volcanic environments.

Geochemistry of rubidium in volcanic environments

Quaternary arc volcanism on the Kamchatka peninsula, Russia, produced a huge volume of basaltic rocks which form numerous large volcanoes and monogenetic volcanic fields. Among the active volcanoes the most well known and studied is the Tolbachik volcanic complex; it is a part of the Klyuchevskaya Volcanic Group in the Central Kamchatka Depression (Churikova *et al.*, 2015a). The Tolbachik complex consists of two stratovolcanoes, extinct Ostry Tolbachik and active Plosky Tolbachik, and a monogenetic volcanic field known as Tolbachinsky Dol. The latter was formed during several eruptions including the Great Fissure Tolbachik Eruption in 1975–76 and the Tolbachik fissure eruption in 2012–2013 (Volynets *et al.*, 2015).

The large volume of erupted lavas due to Tolbachik's recent activity is well studied in terms of their mineralogy and geochemistry, including direct sampling during eruptions (Churikova *et al.*, 2015a). The Tolbachik lavas and scoria consist of basalts and basaltic andesites with subordinate trachybasalts and basaltic trachyandesite. Basalts, on the basis of potassium content, are subdivided into medium- and high-K varieties; another basalt subdivision based on the MgO/Al₂O₃ ratio comprises high-magnesian, high-alumina and intermediate rocks. Published whole-rock geochemical data (e.g. Churikova *et al.*, 2015b; Volynets *et al.*, 2015) show large variations in content of both major and trace elements, e.g. MgO = 2.1–10.7 wt.%, Na₂O = 2.3–4.2 wt.%, K₂O = 0.7–3.1 and Cr = 7–745 ppm. An unusual geochemical feature of the Tolbachik basalts is their enrichment in copper with 100–250 ppm in bulk rock samples (Portnyagin *et al.*, 2015). On multi-element normalising diagrams (relative to N-type mid-ocean ridge basalts) the Tolbachik basaltic rocks show enrichment in large-ion lithophile elements (e.g. Cs, Rb and Ba) and depletion in high-field-strength elements (e.g. Nb or Ta). This is considered to be a typical signature of subduction-related magmas (Churikova *et al.*, 2001). Mineralogy, trace-element geochemistry and data from Sr–Nd–Pb isotopic studies suggest involvement of several components during formation of primary melts including subducted Pacific sediments, oceanic basaltic crust with additional fluid flux from subducted material (Churikova *et al.*, 2001; Portnyagin *et al.*, 2015) and assimilation of ore-bearing hydrothermal veins at the crustal level (Zelenski *et al.*, 2016).

Tolbachik is also well known due to strong fumarolic activity and remarkable mineralogy of fumarolic deposits. They have

been studied since 1976 and hundreds of new minerals with unusual combinations of both abundant and trace elements have been found and described in detail (Vergasova and Filatov, 2012; Pekov *et al.*, 2018a). Particularly abundant are sulfate minerals with Na⁺ and K⁺ as major cations. Other alkaline elements, Rb and Cs, are rare in fumarolic minerals. Yet, some species contain these elements in trace to minor amounts (up to 1.95 wt.% Rb₂O in cesiodymite and 4.11 wt.% Cs₂O in averievite, Pekov *et al.*, 2018b, Vergasova *et al.*, 1998) including cesiodymite that contains Cs as the major constituent (Pekov *et al.*, 2018b).

Rubidium, the element on which this paper is focused, is a trace element in Tolbachik basaltic rocks with concentrations between 13 ppm (primitive high-Mg basalts) and 89 ppm (evolved low-Mg basaltic andesites). Rb_N values (normalised relative to N-MORD) vary from 24 to 159. On Harker-type diagrams, the element exhibits a clear positive correlation with K₂O (Supplementary Fig. 1) and this relationship seems to be common for the Quaternary volcanic rocks from the Kurile–Kamchatka region (Popolitov and Volynets, 1982). In basalts, Rb is likely to be hosted by plagioclase pheno- and microphenocrysts and possibly by the groundmass glass.

Rubidium is also present in high-temperature magmatic gases (1030–1060°C) sampled during the 2012–13 eruption and considered to be uncontaminated. The measured Rb content in condensate was 1.0±0.2 ppm (Zelenski *et al.*, 2014) and 1.7 ppm (Chaplygin *et al.*, 2016). A slightly lower concentration of Rb (0.78 ppm) was measured in the gases of the 1975–1976 eruption (Menyailov and Nikitina, 1980). In contrast, the Rb content in the low-temperature gas (690°C) from the 2012–13 eruption was found to be outstandingly high at 16.5 ppm (Chaplygin *et al.*, 2016). However, the strong enrichment of trace elements in the gas was explained as a secondary feature due to “evaporation at forced pumping during sampling and possible dissolution of earlier precipitated sublimates in the gas conduit” (Chaplygin *et al.*, 2016). Despite the low Rb content in Tolbachik gases, it is essentially above that in gases produced by other volcanoes. For instance, exhalations of Kudryavy, Kurily, Russia; Gorelyi, Kamchatka, Russia; Erta Ale, Afar, Ethiopia; Mount St. Helens, USA; and White Island, New Zealand volcanoes exhibit extremely low Rb content in condensate with values between 0.22 and 0.002 ppm (Tedesco and Toutain, 1991; Symonds and Reed, 1993; Taran *et al.* 1995; Zelenski *et al.*, 2013; Chaplygin *et al.*, 2015). The high enrichment factor for Rb in Tolbachik gases (LogEF_{Rb} = 2–3, Chaplygin *et al.*, 2016; Zelenski *et al.*, 2014) suggests that the element was transported in the form of volatile species from a source and not derived from wall rocks due to contamination.

To date, whole-rock compositional data for basalts with different degrees of alteration by fumarolic gases are still lacking and one can but suggest the tentative mechanisms of gas enrichment by the trace elements to the levels essential for the crystallisation of Rb-enriched minerals. For instance, such strong Rb enrichment could be due to its extraction by hot hydrated gases from the plagioclase and glass, and/or dissolution of some earlier precipitated fumarolic minerals, e.g. sulfates, as suggested by Chaplygin *et al.* (2016). In this case, some helpful data can be collected from the results of model experiments, including chemical composition, structure, formation mechanism (chemical transport, crystallisation from melt, hydration rate etc.) and other features of synthetic Rb-containing species chemically relevant to the currently few known minerals. As yet, rubidium accumulates mostly in the copper sulfate or oxysulfate salts [alumoklyuchevskite,

$K_3Cu_3AlO_2(SO_4)_4$ (Siidra *et al.*, 2017); belousovite, $KZn(SO_4)Cl$ (Siidra *et al.*, 2018a); cesiodymite, $CsKCu_5O(SO_4)_5$ and cryptochalcite, $K_2Cu_5O(SO_4)_5$ (Pekov *et al.*, 2018b); parawulfite, $K_5Na_3Cu_8O_4(SO_4)_8$ and wulfite, $K_3NaCu_4O_2(SO_4)_4$ (Pekov *et al.*, 2014) and in the following two copper vanadates: $(Cu_5O_2)(AsO_4)(VO_4) \cdot (Cu_{0.5} \square_{0.5})Cl$ (Siidra *et al.*, 2019b) and averievite $Cu_5O_2(VO_4)_2 \cdot n(Cs,Rb,K)Cl$ (Vergasova *et al.*, 1998). The current paper reports the results of our further studies of multinary Rb–Cu sulfates where no less than eight new compounds representing four new structure types have been observed.

Experimental

Synthesis

Potassium- and copper-bearing sulfate minerals such as chlorothionite, $K_2Cu(SO_4)Cl_2$, piypite, $K_4Cu_4O_2(SO_4)_4 \cdot (Na,Cu)Cl$ and cryptochalcite, $K_2Cu_5O(SO_4)_5$, were found in fumarolic sublimates, hence the chemical vapour transport method (CVT-method) was chosen due to similarity with natural conditions of mineral formation from volcanic gases. In our case, however, most reactions did not produce essential sublimates therefore the conventional solid-state synthesis (Nekrasova *et al.*, 2021) in evacuated silica tubes was preferred.

Synthesis of $Rb_2Cu(SO_4)Cl_2$ and $Rb_4Cu_4O_2(SO_4)_4 \cdot (Cu_{0.83}Rb_{0.17}Cl)$
Single crystals of $Rb_2Cu(SO_4)Cl_2$ and $Rb_4Cu_4O_2(SO_4)_4 \cdot (Cu_{0.83}Rb_{0.17}Cl)$ were grown by slow cooling of a melt containing anhydrous $CuSO_4$ (Prolabo, 98%) and $RbCl$ (Alfa Aesar, 99%) in the ratio 1:2. The precursors were pre-dried at 200°C for 2 h to remove traces of absorbed water and then mixed rapidly and ground in an agate mortar in air for 5 min. The mixtures were pressed into pellets (ca. 5 mm × 2 mm) and loaded into silica ampoules (ca. 10 cm × 0.8 cm), which were evacuated (10–2 mbar) and sealed. The ampoules were placed horizontally in a tubular furnace and heated up to 700°C over 3 h and kept at 700°C for 10 h. Cooling to 550°C was performed over 72 h, and an additional 12 h was taken to reach room temperature. The products consisted of sky-blue crystals of $Rb_2Cu(SO_4)Cl_2$ and green crystals of $Rb_4Cu_4O_2(SO_4)_4 \cdot (Cu_{0.83}Rb_{0.17}Cl)$ (Fig. 1).

Synthesis of $Rb_2Cu_2(SO_4)_3$ and $Rb_2Cu_5O(SO_4)_5$
Crystals of $Rb_2Cu_2(SO_4)_3$ and $Rb_2Cu_5O(SO_4)_5$ were formed in the same experimental run. Rb_2SO_4 (Sigma-Aldrich, 99.99%) and $CuSO_4$ (Prolabo, 98%) were mixed carefully in an agate mortar in the ratio 3:1, pelletised, and sealed as described above. The ampoule was heated up to 700°C for 3 h, soaked for 10 h, cooled to 500°C in 96 h and further cooled in 12 h to room temperature. The products consisted of green $Rb_2Cu_5O(SO_4)_5$ and sky-blue $Rb_2Cu_2(SO_4)_3$ crystals (Fig. 1).

Synthesis of $Rb_2Cu_2(SO_4)_3(H_2O)$

The new compound $Rb_2Cu_2(SO_4)_3(H_2O)$ was synthesised during a side process. A 3:1 mixture of Rb_2SO_4 (Sigma-Aldrich, 99.99%) and $CuSO_4$ (Prolabo, 98%) was exposed to air for one week. The colour of the mixture turned light blue due to hydration of copper sulfate. The mixture was processed as described above; the ampoule was heated to 750°C in 5 h, soaked for 10 h, then cooled to 500°C over a period of 40 h, after which the furnace was switched off. The products consisted of anhydrous green crystals of $Rb_2Cu_5O(SO_4)_5$ and hydrated light-blue crystals of $Rb_2Cu_2(SO_4)_3(H_2O)$.

Synthesis of $RbMCu(SO_4)_2$ ($M = Na, K, Rb$)

These three new compounds were prepared according to a slightly different protocol. Mixtures of Rb_2SO_4 , Na_2SO_4 , or K_2SO_4 (all pre-heated at 140°C for 3–4 h) and $CuSO_4$ (obtained by dehydration of $CuSO_4 \cdot 5H_2O$ at 450°C for 4 h) were mixed in a 1:1:2 molar ratio, ground, and placed in silica capsules (5 mm inner diameter, 100 mm long). The tubes were evacuated to $3 \cdot 10^{-2}$ Torr, flame sealed and placed in a vertical furnace with ‘cold’ ends protruding out so that any absorbed water would condense therein. The mixtures were annealed first at 350°C for 96 h; the ampoules were opened, inhomogeneous samples re-ground and further annealed at 450–475°C for more 96 h. The samples partially melted and formation of green or blue crystals occurred on cooling.

Though the hygroscopicity of the compounds in discussion was not studied, it is very likely that these compounds would hydrate readily in moist air. High hygroscopicity and rapid hydration was reported for several potassium analogues, e.g. $K_2Cu(SO_4)_2$ (Zhou *et al.*, 2020) and $K_2Cu_2(SO_4)_3$ (Lander *et al.*, 2017); most natural copper sulfate minerals are also unstable in moist air (Siidra *et al.*, 2019a, 2021a). The most likely reason for such behaviour is non-rigidity of the coordination sphere of both alkali cations (due to weak binding to any ligands) and copper (due to the pronounced Jahn–Teller effect). An indirect indication comes from the observation that evacuation of silica tubes containing re-ground samples was relatively slow, most likely due to elimination of water absorbed upon grinding. Nonetheless, the complex sulfates seem to be less hygroscopic compared to $CuSO_4$ and Rb_2SO_4 .

Single-crystal X-ray studies

Single crystals of all the compounds were isolated visually under a binocular microscope and mounted on thin glass fibres for X-ray diffraction analysis using a Bruker APEX II DUO X-ray diffractometer with a micro-focus X-ray tube operated with $MoK\alpha$ radiation at 50 kV and 0.6 mA. The data were integrated and corrected for absorption using a multi-scan type model implemented in the Bruker programs APEX and SADABS (Bruker, 2014). More than a hemisphere of X-ray diffraction data was collected for each crystal. The structure determinations and refinements were performed using SHELXL software (version 2018/3) (Sheldrick, 2015). Crystallographic information for all obtained phases is summarised in Table 1. Atomic coordinates and additional structural information are provided in the crystallographic information files and are available as Supplementary material (see below).

Results

Structures without additional O^{2-} anions.

$Rb_2Cu(SO_4)_2$

Statistics of diffraction intensities and systematic extinctions were consistent with the space group $Pna2_1$. The $|E^2 - 1|$ parameter was equal to 0.668, which clearly indicated high probability of a non-centrosymmetry (NCS) (Marsh, 1995), confirmed by subsequent structure solution and refinement.

The asymmetric unit contains one symmetrically independent Cu^{2+} , two Rb^+ and two S^{6+} cations. All Cu–O bonds ≤ 3.05 Å and Rb–O bonds ≤ 3.55 Å were taken into consideration. The Cu1 atom forms four very strong Cu–O_{eq} bonds (≤ 2 Å) resulting in a CuO_4 square which is complemented by a fifth, longer Cu–

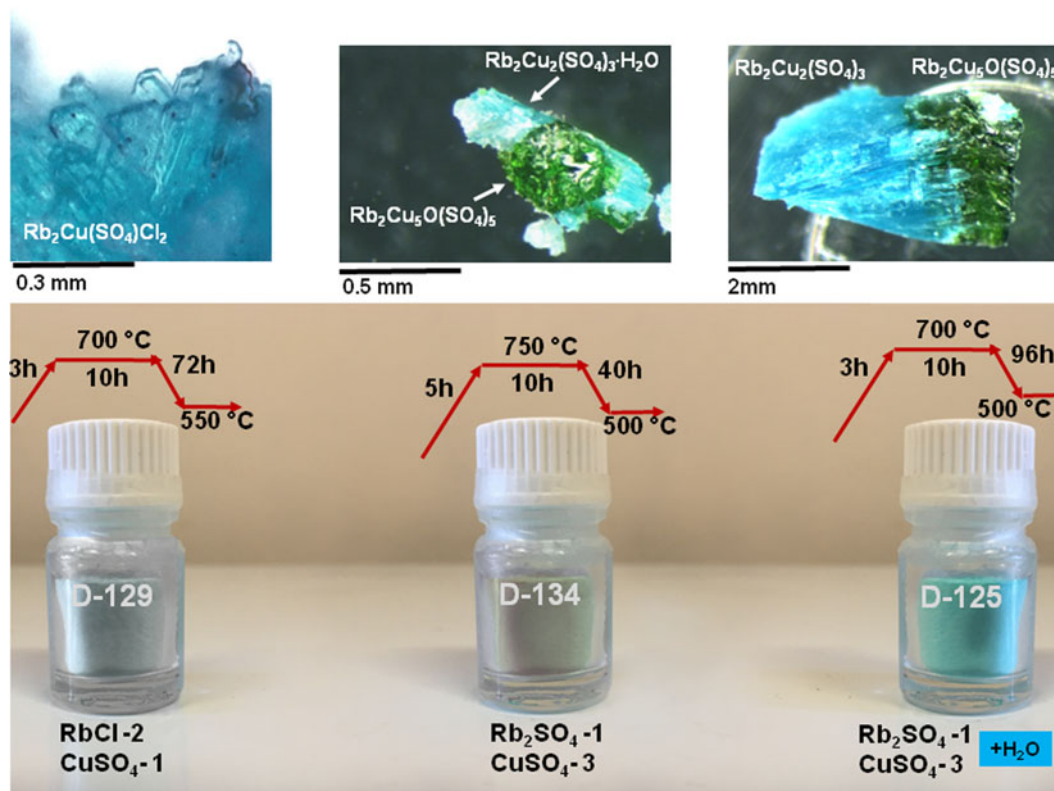


Fig. 1. Crystals of blue $\text{Rb}_2\text{Cu}(\text{SO}_4)\text{Cl}_2$, green $\text{Rb}_2\text{Cu}_5\text{O}(\text{SO}_4)_5$, blue $\text{Rb}_2\text{Cu}_2(\text{SO}_4)_3\cdot\text{H}_2\text{O}$ and $\text{Rb}_2\text{Cu}_2(\text{SO}_4)_3$. Initial reagent mixtures and schemes of the synthesis for each compound are shown.

O_{ap} bond of 2.182 Å, to form a CuO_5 distorted tetragonal pyramid (Fig. 2). The Cu1 atom forms one additional long bond of 2.994(4) Å, resulting in a [4+1+1] CuO_6 octahedron strongly distorted by the Jahn–Teller effect. Such ‘Jahn–Teller’ type of coordination geometry of Cu^{2+} cations is rather common in minerals and inorganic materials (Burns and Hawthorne, 1995).

Both Rb cations centre irregular polyhedra of oxygen atoms (eight vertices for Rb1 atom and nine for Rb2). Each of two S sites centres the respective tetrahedra. The average S–O bond-lengths, 1.47 Å, are consistent with the value of 1.475 Å reported for sulfate minerals (Hawthorne *et al.*, 2000).

The CuO_6 polyhedra share O3–O5 and O4–O5 oxygen edges and O1 and O7 vertices with SO_4 tetrahedra forming clusters depicted in Fig. 2. These are linked into an open framework with a three-dimensional system of channels occupied by the Rb^+ cations. The structural topology of the $[\text{Cu}(\text{SO}_4)_2]^{2-}$ framework in $\text{Rb}_2\text{Cu}(\text{SO}_4)_2$ is unique and has not been observed previously. The projection in the bc plane provides good evidence of the ‘up’ only orientation of all the sulfate groups, along the polar $2_1 c$ -axis, confirming the NCS character of this material.

The Cu1–S1 and Cu1–S2 distances in $\text{Rb}_2\text{Cu}(\text{SO}_4)_2$ are 2.5718(13) Å and 2.9737(12) Å, respectively. In fact, edge sharing between sulfate tetrahedra and transition metal-centred octahedra is rather uncommon. A similarly short Cu–S distance of 2.593 Å is observed in chlorothionite, $\text{K}_2\text{CuCl}_2(\text{SO}_4)$ (Giacovazzo *et al.*, 1976) wherein the CuO_6 octahedron shares an edge with a SO_4 group. Edge sharing has also been observed recently in the complex Zn sulfate majzlanite, $\text{K}_2\text{Na}(\text{ZnNa})\text{Ca}(\text{SO}_4)_4$ (Siidra *et al.*, 2020), with a Zn–S distance of 2.8704(4) Å.

RbNaCu(SO₄)₂ and RbKCu(SO₄)₂

$\text{RbNaCu}(\text{SO}_4)_2$ and $\text{RbKCu}(\text{SO}_4)_2$ are isotypic and crystallise in the monoclinic space group $C2/c$. The lattice parameters given in Table 1 show a strong unit-cell expansion by 7.62% on replacement of Na by K. Both structures contain, in their asymmetric units, one symmetrically independent Cu site, two S sites and three A (A = Rb, K and Na) sites labelled A1 to A3 (Fig. 3).

The Cu^{2+} cation features four Cu–O_{eq} short bonds with distances of ~ 2 Å forming a nearly square-planar coordination. The lengths of the fifth (longer) Cu–O_{ap} differ markedly: 2.236(2) Å in $\text{RbNaCu}(\text{SO}_4)_2$ versus 2.547(3) Å in $\text{RbKCu}(\text{SO}_4)_2$. The effect of the alkali cation size on the Cu^{2+} coordination has been observed before in layered copper hydrogen selenite halides (Charkin *et al.*, 2019). The CuO_5 tetragonal pyramids are complemented by a sixth long and relatively weak bond of 2.604(2) Å and 2.713(3) Å for $\text{RbNaCu}(\text{SO}_4)_2$ and $\text{RbKCu}(\text{SO}_4)_2$, respectively. Thus, the coordination of the Cu^{2+} cation can also be described as [4+1+1].

In contrast to $\text{KNaCu}(\text{SO}_4)_2$ (Borisov *et al.*, 2021), the cation ordering in the rubidium analogue is less perfect. Only the A1 site in the sodium compound is occupied exclusively by Rb^+ while all the other alkali sites demonstrate mixed occupancies as:

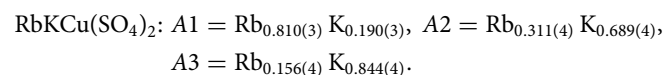
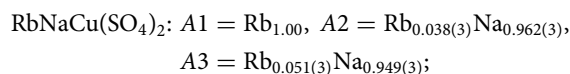


Table 1. Crystallographic data for the new anhydrous alkali copper sulfates.

	Rb ₂ Cu(SO ₄) ₂	RbNaCu(SO ₄) ₂	RbKCu(SO ₄) ₂	Rb ₂ Cu ₂ (SO ₄) ₃	Rb ₂ Cu ₂ (SO ₄) ₃ (H ₂ O)	Rb ₂ Cu(SO ₄)Cl ₂	Rb ₄ Cu ₄ O ₂ (SO ₄) ₄ · (Cu _{0.83} Rb _{0.17} Cl)	Rb ₂ Cu ₅ O(SO ₄) ₅
Crystal system	Orthorhombic	Monoclinic	Monoclinic	Orthorhombic	Monoclinic	Monoclinic	Tetragonal	Triclinic
Space group	<i>Pna</i> 2 ₁	<i>C</i> 2/ <i>c</i>	<i>C</i> 2/ <i>c</i>	<i>P</i> 2 ₁ 2 ₁ 2 ₁	<i>P</i> 2 ₁ / <i>n</i>	<i>C</i> 2/ <i>c</i>	<i>I</i> 4	<i>P</i> $\bar{1}$
Unit-cell dimensions								
<i>a</i> (Å)	9.2521(4)	16.034(3)	16.1865(14)	4.8359(19)	10.1158(9)	7.4645(7)	14.171(14)	10.1002(9)
<i>b</i> (Å)	10.9671(5)	9.560(2)	10.0026(9)	12.294(4)	6.1409(5)	16.0377(18)		12.4740(10)
<i>c</i> (Å)		9.170(2)	9.3923(8)	19.036(7)	20.3446(19)	7.6580(8)	4.991(5)	14.5961(11)
α (°)	8.9612(4)							77.227(4)
β (°)		92.792(6)	92.149(2)		103.564(2)	116.327(6)		81.111(4)
γ (°)								89.880(4)
Unit-cell volume (Å ³)	909.28(7)	1403.9(5)	1519.6(2)	1131.7(7)	1228.56(19)	821.68(15)	1002(2)	1770.9(3)
Calculated density (g·cm ⁻³)	3.116	3.472	3.341	3.441	3.267	3.245	3.695	3.694
Absorption coefficient (mm ⁻¹)	13.507	10.975	10.594	6.885	11.910	15.285	15.752	6.394
Crystal size (mm)	0.10×0.10×0.10	0.11×0.13×0.13	0.14×0.10×0.10	0.10×0.10×0.10	0.13×0.13×0.10	0.13×0.13×0.07	0.08×0.08×0.10	0.08×0.08×0.10
Data collection								
Temperature (K)	296(2)	296(2)	296(2)	296(2)	296(2)	296(2)	296(2)	296(2)
Radiation, wavelength (Å)	MoK α , 0.71073	MoK α , 0.71073	MoK α , 0.71073	MoK α , 0.71073	MoK α , 0.71073	MoK α , 0.71073	MoK α , 0.71073	MoK α , 0.71073
θ range (°)	2.880–27.999	2.481–27.992	2.394–27.635	2.748–18.960	2.059–27.998	2.540–27.989	2.032–30.000	1.322–26.428
<i>h</i> , <i>k</i> , <i>l</i> ranges	–12→12 –14→14 –11→11	–21→21 –12→8 –12→8	–13→20 –12→9 –12→5	–5→5 –13→13 –22→22	–13→8 –8→8 –26→26	–9→9 –21→21 –10→9	–19→19 –19→19 –7→7	–16→15 –19→19 –23→20
Total reflections collected	18,965	6789	3775	5378	11,103	5905	6648	68,695
Unique reflections (<i>R</i> _{int})	2180 (0.04)	1698 (0.02)	1678 (0.02)	1759 (0.09)	2960 (0.05)	990 (0.03)	1455 (0.08)	14,571 (0.09)
Unique reflections <i>F</i> > 4 σ (<i>F</i>)	2049	1586	1387	1296	2005	896	944	7772
Structure refinement								
Weighting coefficients <i>a</i> , <i>b</i>	0.0, 0.0000	0.0176, 5.6518	0.0271, 0.0310	0.0297, 0.0000	0.0471, 3.3470	0.0204, 1.4496	0.0000, 13.7767	0.0421, 0.0000
Data/restraints/parameters	2180/1/123	1698/0/123	1678/0/123	1759/6/174	2960/3/189	990/0/50	1455/67/81	14571/0/596
<i>R</i> ₁ [<i>F</i> > 4 σ (<i>F</i>)], <i>wR</i> ₂ [<i>F</i> > 4 σ (<i>F</i>)]	0.019, 0.043	0.019, 0.046	0.025, 0.057	0.052, 0.091	0.041, 0.091	0.019, 0.044	0.042, 0.064	0.050, 0.097
<i>R</i> ₁ all, <i>wR</i> ₂ all	0.023, 0.045	0.021, 0.047	0.036, 0.061	0.083, 0.103	0.076, 0.107	0.024, 0.046	0.088, 0.077	0.127, 0.127
Gof on <i>F</i> ²	1.009	1.105	1.077	1.014	1.012	1.038	1.041	1.004
Largest diff. peak and hole (e Å ⁻³)	0.41, –0.33	0.60, –0.46	0.44, –0.55	0.98, –0.88	2.39, –1.35	0.58, –0.79	1.07, –0.90	2.31, –1.82

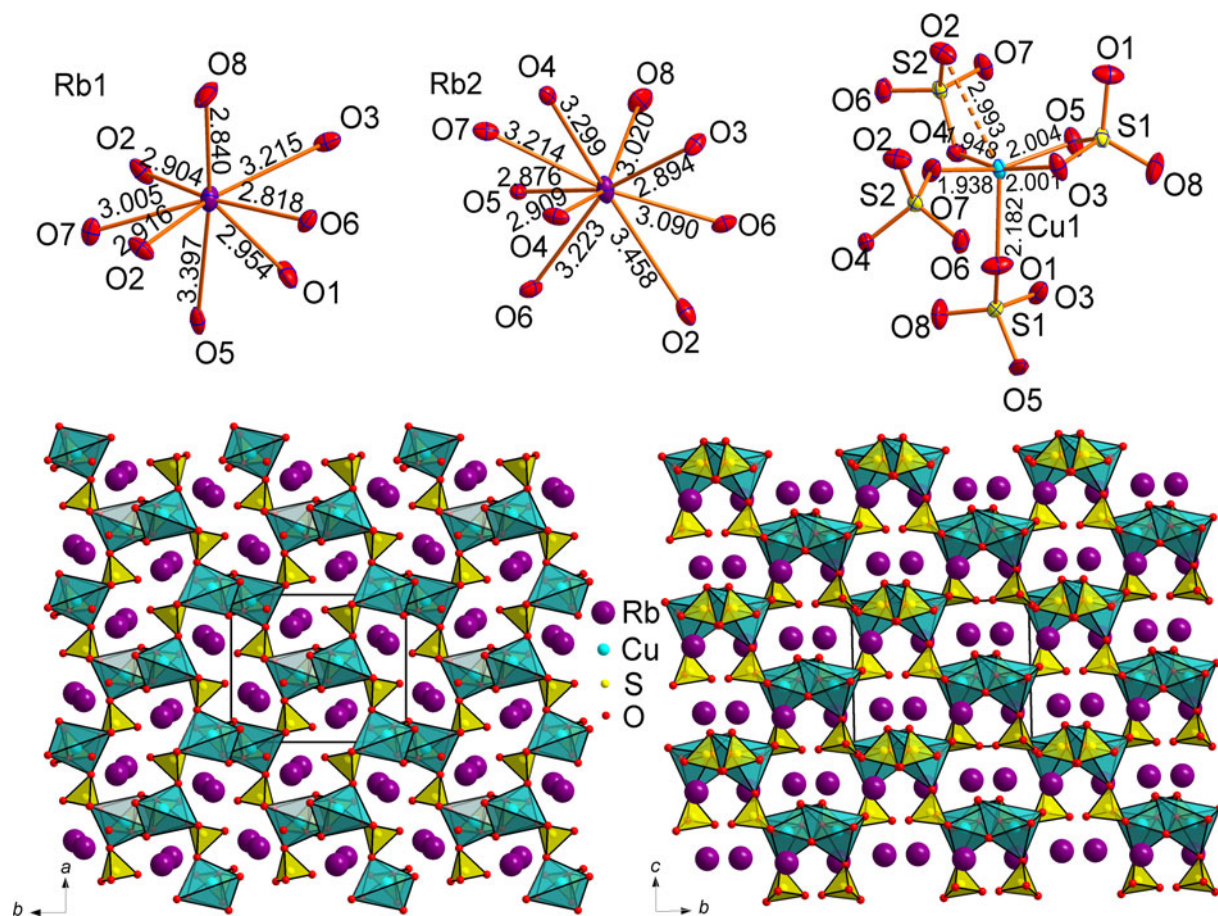


Fig. 2. Coordination environments of Rb^+ , Cu^{2+} and S^{6+} cations (top) in the crystal structure of $\text{Rb}_2\text{Cu}(\text{SO}_4)_2$. General projections of the crystal structure of $\text{Rb}_2\text{Cu}(\text{SO}_4)_2$ along the c and a axis, respectively (bottom).

The A2 and A3 sites in $\text{RbNaCu}(\text{SO}_4)_2$ contain only a minor amount of Rb^+ admixture. The coordination environments for these sites are typical for Na^+ cations (distorted octahedra, Fig. 3), while a CN = 11 for the A1 site is typical for Rb^+ . In $\text{RbKCu}(\text{SO}_4)_2$, the A2 and A3 sites show coordination numbers (CN = 10 for both sites) in accordance with the larger radius of K^+ . In this case, cation disorder is more pronounced which agrees with the smaller relative differences in cation size.

The S atoms are central to approximately regular SO_4 tetrahedra. Akin to $\text{Rb}_2\text{Cu}(\text{SO}_4)_2$, the sulfate moieties share one of the edges with CuO_6 octahedra ($\text{Cu}-\text{S}2 = 2.8315(8)$ Å and $2.8756(11)$ Å for $\text{RbNaCu}(\text{SO}_4)_2$ and $\text{RbKCu}(\text{SO}_4)_2$, respectively) (Fig. 3), despite unfavourable repulsive interactions between Cu^{2+} and S^{6+} .

$\text{RbNaCu}(\text{SO}_4)_2$ and $\text{RbKCu}(\text{SO}_4)_2$ are formally isostructural to the recently reported $\text{KNaCu}(\text{SO}_4)_2$ (Borisov *et al.*, 2021) and $\text{K}_2\text{Cu}(\text{SO}_4)_2$ (Zhou *et al.*, 2020), although some differences in the cation coordinations are clearly visible. The SO_4 tetrahedra and the CuO_6 polyhedra form the porous $[\text{Cu}(\text{SO}_4)_2]^{2-}$ framework with two types of channels parallel to the c axis. The larger (elliptical) channels are occupied preferably by larger Rb^+ (A1 sites), whereas the smaller ones are filled mostly by Na^+ (in $\text{RbNaCu}(\text{SO}_4)_2$) or K^+ (in $\text{RbKCu}(\text{SO}_4)_2$). Note the complete size-based ordering of alkali cations in $\text{KNaCu}(\text{SO}_4)_2$ (Borisov *et al.*, 2021), which is somewhat less pronounced in its Rb-based analogues.

$\text{Rb}_2\text{Cu}_2(\text{SO}_4)_3$

The crystal structure of another new anhydrous sulfate, $\text{Rb}_2\text{Cu}_2(\text{SO}_4)_3$ with langbeinite-type $A_2^+M_2^{2+}(\text{SO}_4)_3$ stoichiometry (Table 1) contains two symmetrically independent Rb sites, two Cu sites and three S atoms (Fig. 4).

In $\text{Rb}_2\text{Cu}_2(\text{SO}_4)_3$, Rb^+ and S^{6+} cations have typical coordination environments, similar to the aforementioned, whereas the coordination of the Cu^{2+} cations demonstrate interesting features worthy of discussion. The Cu1 atom has four short and strong $\text{Cu}-\text{O}_{\text{eq}}$ bonds thus forming CuO_4 squares. However, it has three additional very long $\text{Cu1}-\text{O}5 = 2.864(12)$, $\text{Cu1}-\text{O}1 = 2.925(15)$ Å and $\text{Cu1}-\text{O}10 = 2.981(15)$ Å bonds, thus forming CuO_7 [4+3] coordination environments. These $\text{Cu}-\text{O}$ bonds have bond-valence contributions of 0.04–0.03 valence units and thus should be taken into consideration. The Cu2 atom has CuO_6 [4+1+1] coordination environments, as in $\text{Rb}_2\text{Cu}(\text{SO}_4)_2$ described above. Both the CuO_6 and CuO_7 polyhedra demonstrate bidentate bridging with SO_4 tetrahedra.

$\text{Rb}_2\text{Cu}_2(\text{SO}_4)_3$ is isostructural to $\text{K}_2\text{Cu}_2(\text{SO}_4)_3$ described by Lander *et al.* (2017). The Cu-centred polyhedra and SO_4 tetrahedra form $[\text{Cu}_2(\text{SO}_4)_3]^{2-}$ ribbons depicted in Fig. 4. The arrangement of sulfate tetrahedra and Cu-centred polyhedra was originally described by Lander *et al.* (2017) as a herringbone pattern.

$\text{Rb}_2\text{Cu}_2(\text{SO}_4)_3(\text{H}_2\text{O})$ ‘hydrolangbeinite’

The dominant motif of the novel $\text{Rb}_2\text{Cu}_2(\text{SO}_4)_3(\text{H}_2\text{O})$ structure are layers formed by the corner-sharing and edge-sharing

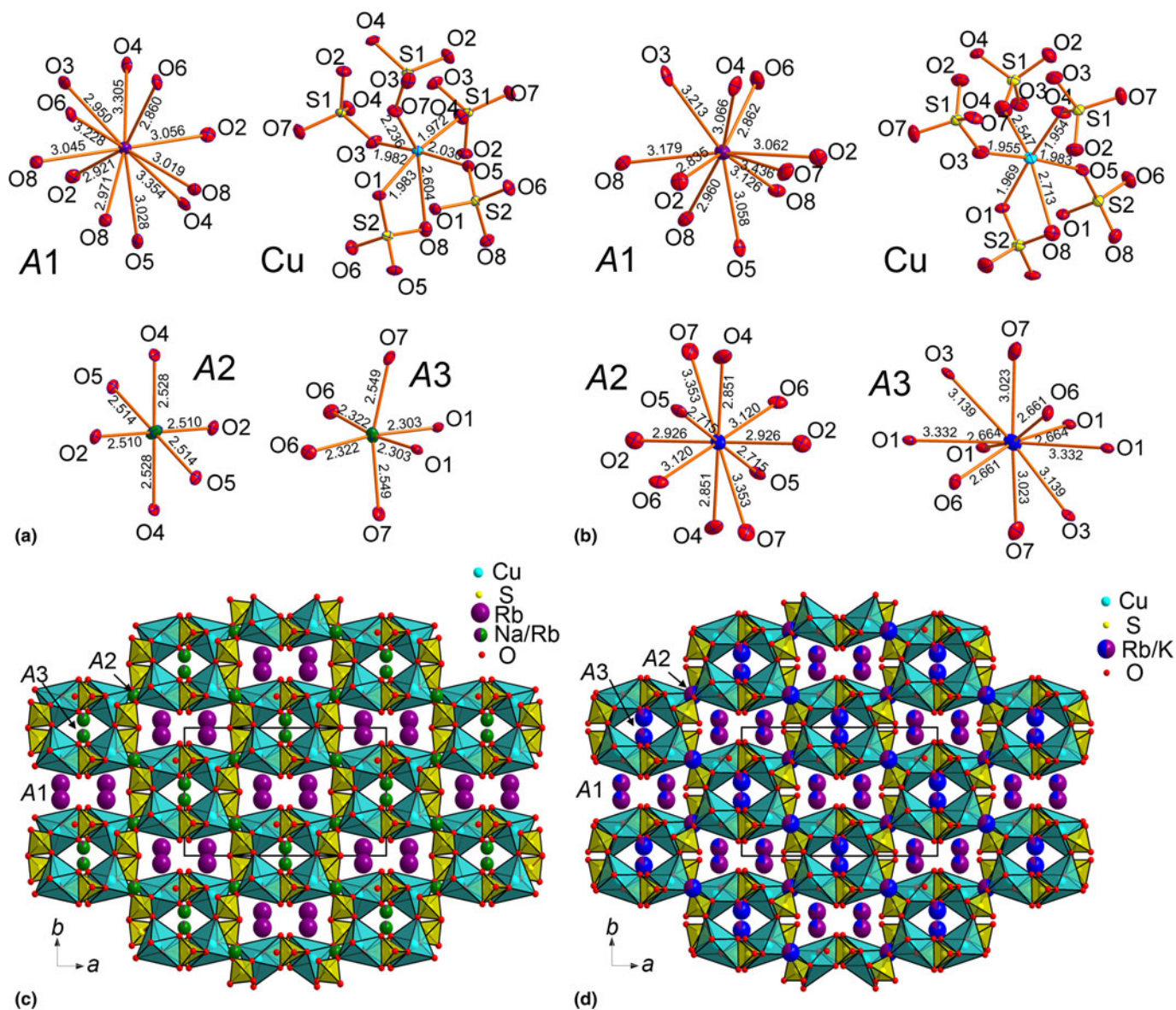


Fig. 3. Coordination environments of A^+ ($A = \text{Rb}, \text{K}$ and Na), Cu^{2+} and S^{6+} cations in the crystal structures of $\text{RbNaCu}(\text{SO}_4)_2$ (a) and $\text{RbKCu}(\text{SO}_4)_2$ (b). General projections of the crystal structure of $\text{RbNaCu}(\text{SO}_4)_2$ (c) and $\text{RbKCu}(\text{SO}_4)_2$ (d) along the c axis.

between sulfate tetrahedra and Cu–O polyhedra (Fig. 5). The $[\text{Cu}_2(\text{SO}_4)_3(\text{H}_2\text{O})]^{2-}$ layers are parallel to the ab plane. In general, a layered character is typical for hydrated copper oxysalt structures. In $\text{Rb}_2\text{Cu}_2(\text{SO}_4)_3(\text{H}_2\text{O})$, the layers are linked together by Rb1 and Rb2 atoms coordinated by eight and ten oxygen atoms, respectively. Note that water molecules are bonded exclusively to Rb1 atoms. The Cu1 site shows a typical coordination with the formation of CuO_5 tetragonal pyramids with an almost planar CuO_4 base. The Cu2-centred CuO_6 octahedron demonstrates an exceptionally strongly distorted character. Cu2–O5 and Cu2–O6 bonds are strongly inclined (Fig. 5) relative to the equatorial plane of octahedron. This distortion is again due to the edge-sharing through O5–O6 with the S_2O_4 tetrahedron. The topology of the $[\text{Cu}_2(\text{SO}_4)_3(\text{H}_2\text{O})]^{2-}$ layer is somewhat similar to that one for the $[\text{Cu}_2(\text{SO}_4)_3]^{2-}$ ribbons in anhydrous $\text{Rb}_2\text{Cu}_2(\text{SO}_4)_3$ (Fig. 4). The rearrangement of sulfate groups in $\text{Rb}_2\text{Cu}_2(\text{SO}_4)_3(\text{H}_2\text{O})$ is provoked by the hydration of

one of the Cu-centred polyhedra. The vertex occupied by the water molecule is unshared and projected into the interlayer space.

$\text{Rb}_2\text{Cu}(\text{SO}_4)\text{Cl}_2$

The coordination environments of atoms in monoclinic ($C2/c$) $\text{Rb}_2\text{Cu}(\text{SO}_4)\text{Cl}_2$ are very similar to those described earlier in its natural K-analogue, chlorothionite, $\text{K}_2\text{Cu}(\text{SO}_4)\text{Cl}_2$ (Giacovazzo *et al.*, 1976) crystallising in the orthorhombic space group $Pnma$. The Cu atom shows mixed-ligand coordination environments with oxygen and chlorine atoms, thus forming CuO_2Cl_2 coordination environments complemented by the two very long Cu–Cl bonds of 3.2020(8) Å (Fig. 6). These Cu–Cl bonds are much shorter in chlorothionite (3.0467(2) Å). The SO_4 tetrahedra in $\text{Rb}_2\text{Cu}(\text{SO}_4)\text{Cl}_2$ and chlorothionite show very similar S–O bond length values. Two symmetrically independent Rb atoms have strongly dissimilar coordination environments: $\text{Rb1O}_4\text{Cl}_4$ and Rb2O_4 . Rb2 has two Rb–Cl distances of 3.6652(10) Å and

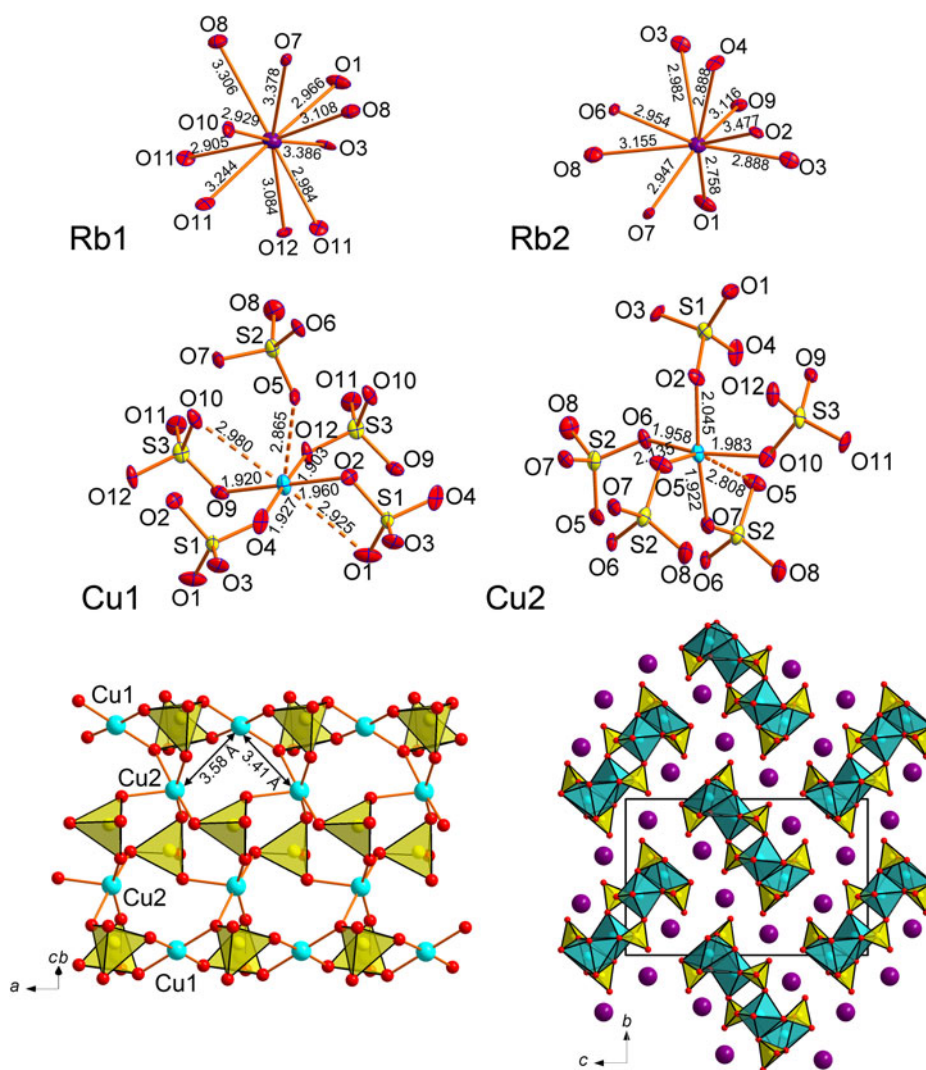


Fig. 4. Coordination environments of Rb^+ , Cu^{2+} and S^{6+} cations (top) in the crystal structure of $\text{Rb}_2\text{Cu}_2(\text{SO}_4)_3$. $[\text{Cu}_2(\text{SO}_4)_3]^{2-}$ ribbon (only short and strong Cu–O bonds are shown) (bottom left) and general projection of the crystal structure of $\text{Rb}_2\text{Cu}_2(\text{SO}_4)_3$ along the a axis (bottom right).

two of 3.6908(9) Å which are beyond the limit of 3.55 Å for the consideration of bonds. Also note the unusually low coordination number of K in chlorothionite.

In $\text{Rb}_2\text{Cu}(\text{SO}_4)\text{Cl}_2$, the main structural feature of edge-sharing between sulfate tetrahedra and CuO_2Cl_4 octahedra remains intact. The Cu–S1 distances are 2.5785(10) Å and 2.593(1) Å in $\text{Rb}_2\text{Cu}(\text{SO}_4)\text{Cl}_2$ and chlorothionite, respectively.

The observed symmetry lowering in $\text{Rb}_2\text{Cu}(\text{SO}_4)\text{Cl}_2$ compared to $\text{K}_2\text{Cu}(\text{SO}_4)\text{Cl}_2$ is probably due to the replacement of K^+ by the larger Rb^+ . This also causes a significant elongation of Cu–Cl bonds in the CuO_4Cl_2 octahedra.

Structures with additional O^{2-} anions

$\text{Rb}_4\text{Cu}_4\text{O}_2(\text{SO}_4)_4 \cdot (\text{Cu}_{0.83}\text{Rb}_{0.17}\text{Cl})$, rubidium analogue of piypite
Piypite, $\text{K}_4\text{Cu}_4\text{O}_2(\text{SO}_4)_4 \cdot (\text{Na,Cu})\text{Cl}$, was described from the fumaroles of the Second scoria cone by Vergasova *et al.* (1984). The crystal structure was solved ($R_1 = 0.035$) using a sample of ‘caratiite’ from Mount Vesuvius, Naples, Italy, by Effenberger and Zemmann (1984). It belongs to the tetragonal symmetry, $I4$, with $a = 13.60(2)$ Å, $c = 4.98(1)$ Å and $V = 921.1$ Å³. Later, Kahlenberg *et al.* (2000) solved the structure ($R_1 = 0.028$) of its

synthetic sodium analogue, $\text{Na}_4\text{Cu}_4\text{O}_2(\text{SO}_4)_4 \cdot (M\text{Cl})$ ($M = \text{Na, Cu, } \square$) in a supercell with $P4/n$, $a = 18.451(1)$, $c = 4.9520(2)$ and $V = 1685.86$ Å³.

The new compound $\text{Rb}_4\text{Cu}_4\text{O}_2(\text{SO}_4)_4 \cdot (\text{Cu}_{0.83}\text{Rb}_{0.17}\text{Cl})$ crystallises analogous to the potassium compound in space group $I4$, $a = 14.171(14)$, $c = 4.991(5)$, $V = 1002(2)$ Å³ and $R_1 = 0.043$. Proceeding from K to Rb, the value of the a parameter is affected most. We observed no indication of the supercell suggested by Kahlenberg *et al.* (2000). In the structure of $\text{Rb}_4\text{Cu}_4\text{O}_2(\text{SO}_4)_4 \cdot (\text{Cu}_{0.83}\text{Rb}_{0.17}\text{Cl})$, chlorine is disordered over two Cl1A (site occupation factor (s.o.f.) = 0.44(7)) and Cl1B (s.o.f. = 0.55(7)) sites with Cl1A–Cl1B = 0.82(2) Å. All of the atoms except ClA were refined anisotropically.

The structure of $\text{Rb}_4\text{Cu}_4\text{O}_2(\text{SO}_4)_4 \cdot (\text{Cu}_{0.83}\text{Rb}_{0.17}\text{Cl})$ (Fig. 7) contains one symmetrically unique Rb position, one Cu, one S, and one mixed metal site M , occupied by Cu^+ and Rb^+ cations in a ratio indicated above. The Rb^+ cation is coordinated by seven O atoms and two Cl atoms. The Cu site is coordinated by four oxygens forming a distorted CuO_4 square complemented by one apical O^{2-} anion at a distance of 2.395(8) Å and another one at 3.086(11) Å. As a result, an essentially elongated CuO_6 octahedron is formed.

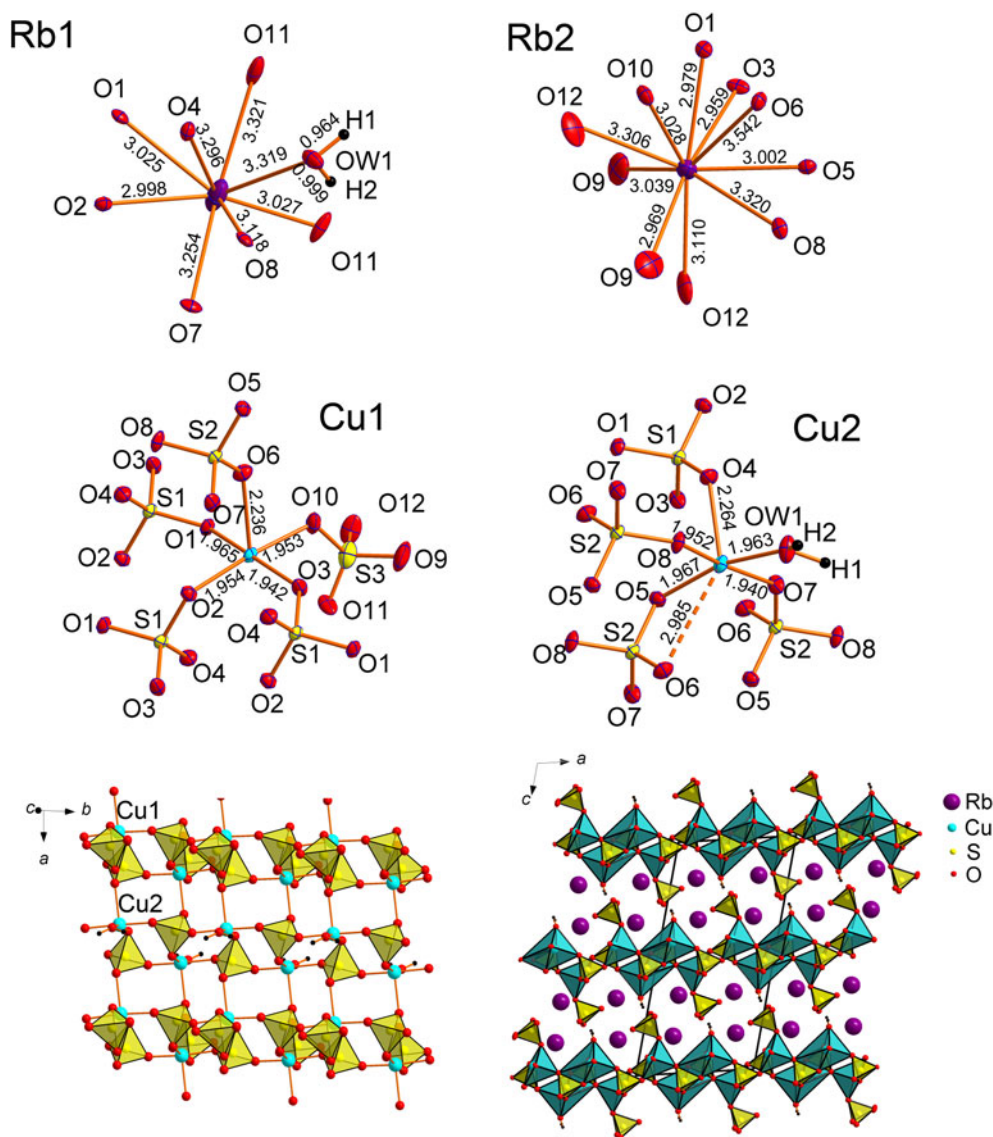


Fig. 5. Coordination environments of Rb^+ , Cu^{2+} and S^{6+} cations (top) in the crystal structure of $\text{Rb}_2\text{Cu}_2(\text{SO}_4)_3(\text{H}_2\text{O})$. $[\text{Cu}_2(\text{SO}_4)_3(\text{H}_2\text{O})]^{2-}$ layer (only short and strong Cu–O bonds are shown) (bottom left) and general projection of the crystal structure of $\text{Rb}_2\text{Cu}_2(\text{SO}_4)_3(\text{H}_2\text{O})$ along the b axis (bottom right).

The mixed M site has a refined occupancy of $\text{Cu}_{0.83(7)}\text{Rb}_{0.17(7)}$. There are two strong bonds to the Cl atoms ($M\text{--Cl1A} = 2.08(5)$ Å and $M\text{--Cl1B} = 2.09(3)$ Å) which correspond to a typical linear Cu^+Cl_2^- anion. There are also four equivalent $M\text{--O2}$ distances of $2.900(9)$ Å that correspond to $\text{Rb}\text{--O}$ bonds.

The O1, O2, O3 and O4 atoms constitute the tetrahedral SO_4^{2-} groups and are further designated as O_t . The ‘additional’ O5 oxygen atom is bonded exclusively to the Cu^{2+} cations (Fig. 7) and is designated as O_a . The $\text{Cu}^{2+}\text{--O}_a$ distances vary in the range of $1.908(15)\text{--}1.922(15)$ Å, whereas $\text{Cu}^{2+}\text{--O}_t$ ranges from $1.908(15)$ to $3.086(11)$ Å. Because of the higher strength of the $\text{Cu}\text{--O}_a$ bonds compared to the weaker $\text{Cu}\text{--O}_t$ bonds, one can describe the copper–oxide substructure of $\text{Rb}_4\text{Cu}_4\text{O}_2(\text{SO}_4)_4 \cdot (\text{Cu}_{0.83}\text{Rb}_{0.17}\text{Cl})$ in terms of oxocentred OCu_4^{2+} tetrahedra.

These tetrahedra link together via common edges to form $[\text{Cu}_2\text{O}]^{2+}$ single chains (Fig. 7). In such units, each tetrahedron shares two of six edges with adjacent tetrahedra. The $[\text{Cu}_2\text{O}]^{2+}$ single chains extend along the c axis. The chains are surrounded by

SO_4 tetrahedra in a rod-like arrangement. Rb^+ cations fill the space in between the rods. In turn, the channels filled by CuCl_2^- linear complexes are formed between the rubidium atoms. Formation of ‘guest’ metal-chloride species with Cu^+ cations in the channels is characteristic for fumarolic minerals: averievite, $\text{Cu}_5\text{O}_2(\text{VO}_4) \cdot n\text{MCl}_x$ ($M = \text{Cu}, \text{Cs}, \text{Rb}$ and K) (Vergasova *et al.*, 1998; Korniyakov *et al.*, 2021) and aleutite, $\text{Cu}_5\text{O}_2(\text{AsO}_4)(\text{VO}_4) \cdot (\text{Cu}_{0.5}\square_{0.5})\text{Cl}$ (Siidra *et al.*, 2019b). A similar phenomenon was observed in the family of copper-lead selenite bromides (Siidra *et al.* 2018b): the oxocentred $\text{OCu}^{2+}_n\text{Pb}_{4-n}$ tetrahedra were present only in the structures containing both Cu^{2+} and Cu^+ . Whenever Cu^{2+} was the sole copper species, the anionic sublattice was formed only by SeO_3^{2-} and Br^- with no ‘extra’ O^{2-} present. A possible explanation, which evidently needs to be further verified, is that the Cu^+ forms strong covalent bonds to the halide anions. The terminal atoms of the strong halo- and/or oxoanions form weaker bonds to the dications (Pb^{2+} or Cu^{2+}), and the ‘extra’ O^{2-} anions are one of the ways to complete their bond-valence sums to saturation.

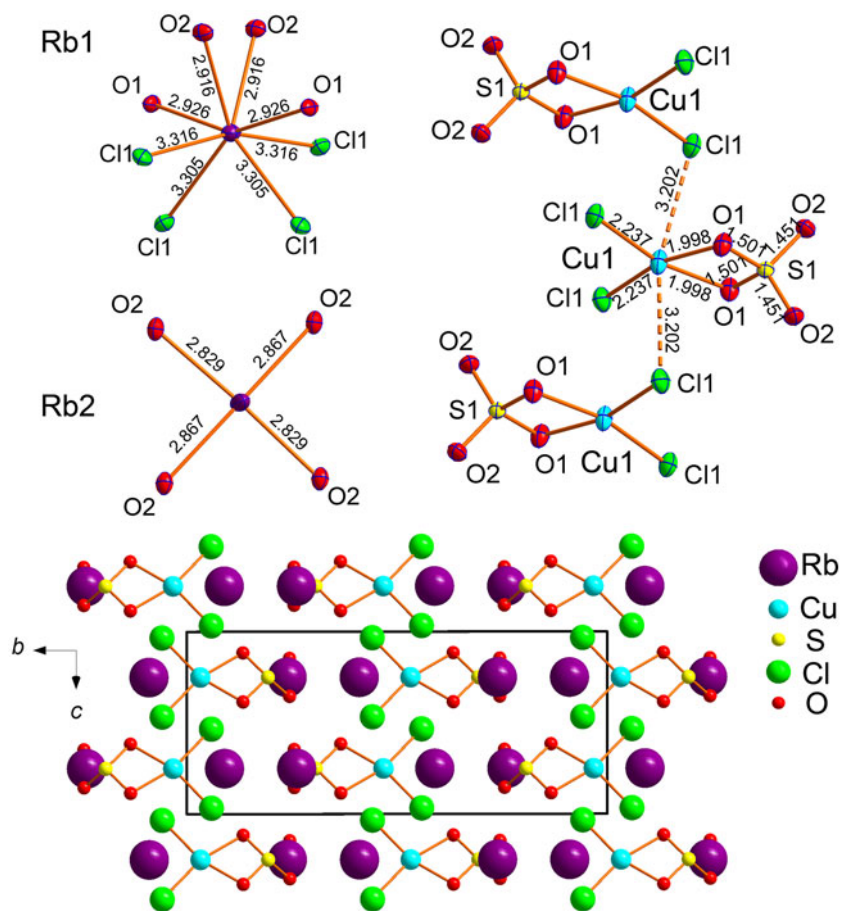


Fig. 6. Coordination environments of Rb^+ , Cu^{2+} and S^{6+} cations (top) in the crystal structure of $\text{Rb}_2\text{Cu}(\text{SO}_4)\text{Cl}_2$. General projection of the crystal structure of $\text{Rb}_2\text{Cu}(\text{SO}_4)\text{Cl}_2$ along the a axis (bottom). Weak and long Cu–Cl bonds are not shown for clarity.

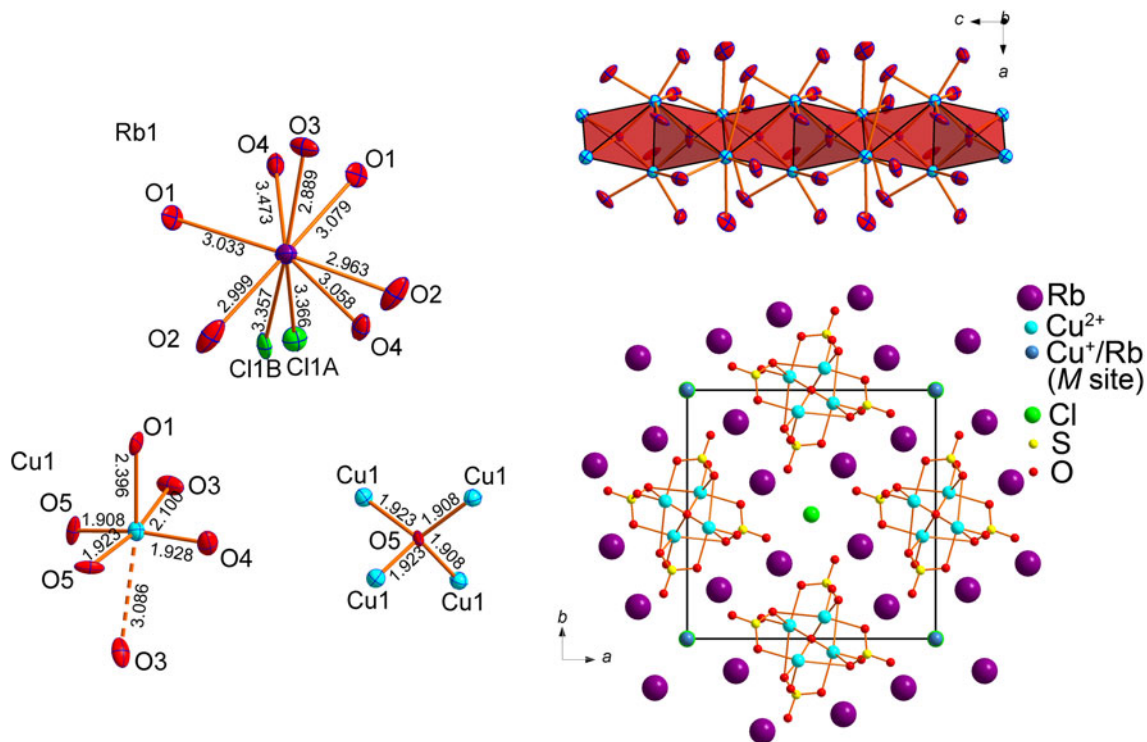


Fig. 7. Coordination environments of Rb^+ , Cu^{2+} cations and additional O^{2-} anions in the crystal structure of $\text{Rb}_4\text{Cu}_4\text{O}_2(\text{SO}_4)_4 \cdot (\text{Cu}_{0.83}\text{Rb}_{0.17}\text{Cl})$ (left). Polyhedral representation of the oxocentred $[\text{Cu}_2\text{O}]^{2+}$ chains surrounded by the oxygen atoms of sulfate groups (top right). General projection of the crystal structure of $\text{Rb}_4\text{Cu}_4\text{O}_2(\text{SO}_4)_4 \cdot (\text{Cu}_{0.83}\text{Rb}_{0.17}\text{Cl})$ along the c axis (bottom right) (Rb–Cl, M–Cl and M–O bonds are omitted for clarity).

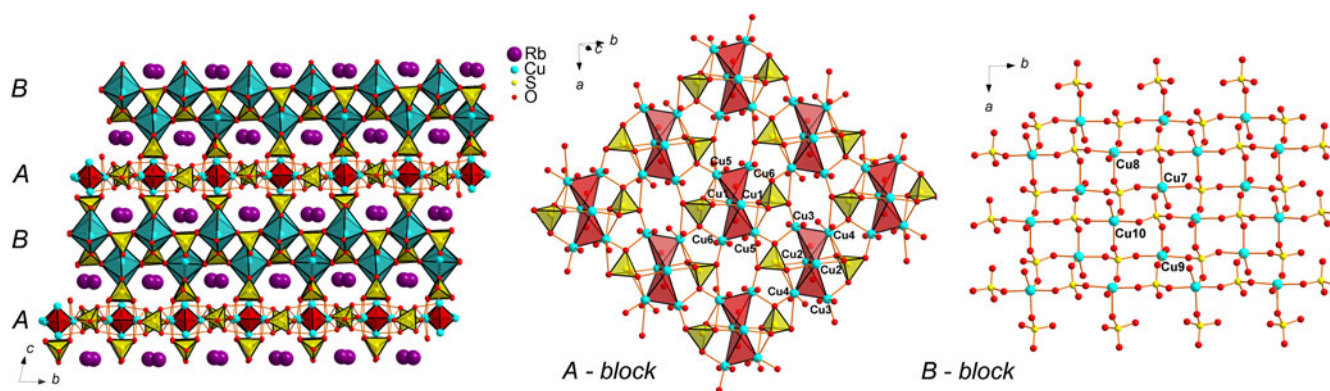


Fig. 8. General projection of the crystal structure of $\text{Rb}_2\text{Cu}_5\text{O}(\text{SO}_4)_5$ along the a axis. The $[\text{Cu}_5\text{O}(\text{SO}_4)_5]^{2-}$ open framework can be described as consisting of two types of blocks, A and B. A-blocks (centre) are formed by O_2Cu_6 dimeric units and sulfate tetrahedra, whereas B-blocks (right) are formed by CuO_5 tetragonal pyramids and sulfate tetrahedra. Rb–O bonds are omitted for clarity.

$\text{Rb}_2\text{Cu}_5\text{O}(\text{SO}_4)_5$, rubidium analogue of cryptochalcite and cesiodymite

$\text{Rb}_2\text{Cu}_5\text{O}(\text{SO}_4)_5$ is isostructural to the recently described cryptochalcite, $\text{K}_2\text{Cu}_5\text{O}(\text{SO}_4)_5$, and cesiodymite, $\text{CsKCu}_5\text{O}(\text{SO}_4)_5$ (Pekov *et al.*, 2018b). Note that both these fumarolic minerals contain significant amounts of Rb (up to 1.95 wt.% Rb_2O). The new compound $\text{Rb}_2\text{Cu}_5\text{O}(\text{SO}_4)_5$ is the first synthetic representative of this structure type. The initial model started from the atomic coordinates provided by Pekov *et al.* (2018b). The unit-cell volume of $\text{Rb}_2\text{Cu}_5\text{O}(\text{SO}_4)_5$ ($V = 1770.9(3) \text{ \AA}^3$) is nearly halfway between those of cryptochalcite ($V = 1751.73(10) \text{ \AA}^3$) and cesiodymite ($V = 1797.52(16) \text{ \AA}^3$). The structure of cryptochalcite-type compounds, and $\text{Rb}_2\text{Cu}_5\text{O}(\text{SO}_4)_5$ in particular, represents an interesting example of the framework formed by both CuO_n polyhedra and oxocentred OCu_4 tetrahedra. The $[\text{Cu}_5\text{O}(\text{SO}_4)_5]^{2-}$ open framework, with Rb^+ in the channels, can be described as consisting of two types of alternating blocks, A and B (Fig. 8). The A-blocks (in the middle) are formed by O_2Cu_6 dimeric units and sulfate tetrahedra, whereas B-blocks (right) are formed by CuO_5 tetragonal pyramids and sulfate tetrahedra.

Discussion and concluding remarks

The compounds reported for the first time and the determination of their crystal structures significantly expand the family of anhydrous copper sulfates. Some of the obtained anhydrous rubidium copper sulfates turned out to be isostructural to known compounds and minerals. An example of this is $\text{Rb}_2\text{Cu}_5\text{O}(\text{SO}_4)_5$, which is isostructural to cesiodymite, $\text{CsKCu}_5\text{O}(\text{SO}_4)_5$ and cryptochalcite, $\text{K}_2\text{Cu}_5\text{O}(\text{SO}_4)_5$ (Table 2). This fact, as well as the high contents of rubidium in natural samples, shows that the discovery of a mineral species with an alkali position, occupied essentially or even predominantly by rubidium, is highly probable. Our synthesis of a number of mineral analogues also demonstrates the possibility of introducing rubidium cations into the already known structural architectures. A slight symmetry lowering, with most structural features left intact, is observed for the Rb-analogue of chlorothionite.

In addition, the minerals and synthetic framework compounds of the $\text{A}_2\text{Cu}(\text{SO}_4)_2$ series demonstrate a vivid example of morphotropism with the formation of structural types depending on the size of the cations residing in the cavities of the $[\text{Cu}(\text{SO}_4)_2]^{2-}$ open framework. To date, five types can be distinguished

Table 2. Crystallographic parameters of known cryptochalcite-type $\text{A}_2[\text{Cu}_5\text{O}(\text{SO}_4)_5]$ compounds.

Mineral/ Synthetic Formula	Cryptochalcite $\text{K}_2[\text{Cu}_5\text{O}(\text{SO}_4)_5]$	Cesiodymite $\text{CsK}[\text{Cu}_5\text{O}(\text{SO}_4)_5]$	Synthetic $\text{Rb}_2[\text{Cu}_5\text{O}(\text{SO}_4)_5]$
Space group	$P\bar{1}$	$P\bar{1}$	$P\bar{1}$
a (Å)	10.0045(3)	10.0682(4)	10.1002(9)
b (Å)	12.6663(4)	12.7860(7)	12.4740(10)
c (Å)	14.4397(5)	14.5486(8)	14.5961(11)
α (°)	102.194(3)	102.038(5)	77.227(4)
β (°)	101.372(3)	100.847(4)	81.111(4)
γ (°)	90.008(3)	89.956(4)	89.880(4)
V (Å ³)	1751.7(1)	1797.5(2)	1770.9(3)
R_1	0.050	0.090	0.050
Reference	Pekov <i>et al.</i> (2018b)	Pekov <i>et al.</i> (2018b)	this work

(Table 3). We propose to call this series of compounds ‘saranchinaite-type’, as the stoichiometry $\text{A}_2\text{Cu}(\text{SO}_4)_2$ was first encountered during the discovery and description of saranchinaite $\text{Na}_2\text{Cu}(\text{SO}_4)_2$ (Siidra *et al.*, 2018c) and shortly thereafter its synthetic analogue (Kovrugin *et al.*, 2019). Saranchinaite forms a framework with a unique topology (further denoted as type α) that has not been identified in other anhydrous copper and alkali metal sulfates. Note the presence of only a minor admixture of potassium in one of the positions in the mineral (Siidra *et al.* 2018c). $\text{K}(\text{Na,K})\text{Na}_2[\text{Cu}_2(\text{SO}_4)_4]$ (Siidra *et al.*, 2021b) crystallises in a completely different structure type (β). The compound $\text{Rb}_2\text{Cu}(\text{SO}_4)_2$ described in this work also forms a new structure type, which we term δ . The recently described family of compounds $\text{KMCu}(\text{SO}_4)_2$ ($M = \text{Na}, \text{K}$) (Borisov *et al.*, 2021; Zhou *et al.*, 2020) is substantially supplemented by two rubidium representatives, $\text{RbNaCu}(\text{SO}_4)_2$ and $\text{RbKCu}(\text{SO}_4)_2$. Attempts to obtain a solely sodium-bearing example of this structural type (γ) were unsuccessful. Sodium analogues of anhydrous sulfates discussed herein, except of chlorothionite, represent their own structure types. However, euchlorine-type $\text{A}_2\text{Cu}_3\text{O}(\text{SO}_4)_3$ ($\text{A}_2 = \text{Na}_2, \text{NaK}$ and K_2) compounds (Nekrasova *et al.*, 2020) and minerals (Vergasova *et al.*, 1988; Siidra *et al.*, 2017, 2019a) crystallise in the same structure type. Framework compounds such as e.g. saranchinaite-type and cryptochalcite-type sulfates may show different architectures depending on the size of the alkali metal, whereas e.g. euchlorine- and chlorothionite-type

Table 3. Crystallographic parameters of known saranchinaite-type $A_2[Cu(SO_4)_2]$ compounds.

Phase type	α -type				β -type	
	Saranchinaite		Synthetic		Synthetic	
Mineral/synthetic	Saranchinaite		Synthetic		Synthetic	
Formula	$Na_2[Cu(SO_4)_2]$		$Na_2[Cu(SO_4)_2]$		$K(Na,K)Na_2[Cu_2(SO_4)_4]$	
Space group	$P2_1$		$P2_1$		$P2_1/c$	
a (Å)	9.0109(5)		8.9711(3)		12.5085(9)	
b (Å)	15.6355(8)		15.5482(5)		9.3166(7)	
c (Å)	10.1507(5)		10.1421(3)		12.7894(10)	
β (°)	107.079(2)		107.155(1)		107.775(2)	
V (Å ³)	1367.06(12)		1351.73(7)		1419.28(19)	
R_1	0.030		0.020		0.030	
Reference	Siidra <i>et al.</i> (2018c)		Kovrugin <i>et al.</i> (2019)		Siidra <i>et al.</i> (2021b)	

Phase type	γ -type				δ -type	ϵ -type
	Synthetic	Synthetic	Synthetic	Synthetic	Synthetic	Synthetic
Mineral/synthetic	Synthetic		Synthetic		Synthetic	Synthetic
Formula	$KNa[Cu(SO_4)_2]$		$K_2[Cu_2(SO_4)_2]$		$RbNa[Cu(SO_4)_2]$	$RbK[Cu(SO_4)_2]$
Space group	$C2/c$		$C2/c$		$C2/c$	$Pna2_1$
a (Å)	15.9721(10)		16.0433(11)		16.034(3)	16.1865(14)
b (Å)	9.4576(6)		9.7819(7)		9.560(2)	10.0026(9)
c (Å)	9.0679(6)		9.2341(7)		9.170(2)	9.3923(8)
β (°)	93.6350(10)		93.2680(10)		92.792(6)	92.149(2)
V (Å ³)	1367.02(15)		1446.79(18)		1403.9(5)	1519.6(2)
R_1	0.029		0.017		0.030	0.025
Reference	Borisov <i>et al.</i> (2021)		Zhou <i>et al.</i> (2020)		this work	this work

sulfates having layered and chain structures are more flexible and can include alkali metals of quite different ionic radii.

Note that the structural architectures of anhydrous sulfates do not relate exclusively to framework ones. Thus, piypite and its synthetic analogues are based on chain copper oxide–sulfate complexes; chlorothionite and its polymorphs are also based on chain complexes formed via weak Cu–Cl bonds. The discovery of a new $Rb_2Cu(SO_4)Cl_2$ monoclinic polymorph of chlorothionite (Table 4) seems to be of particular interest considering the recently discovered interesting magnetic properties of synthetic $K_2Cu(SO_4)_2$ ($X = Cl, Br$) (Soldatov *et al.*, 2018; Bo *et al.*, 2020) and $Na_2Cu(SO_4)Cl_2$ (Fujihala *et al.*, 2020). Note that both sodium and potassium analogues are strictly isostructural. An interesting pattern with a change in symmetry depending on the size of the alkaline cation is observed in the structures of piypite and its synthetic analogues (Table 5). $Rb_4Cu_4O_2(SO_4)_4 \cdot (Cu_{0.83}^{+}Rb_{0.17}Cl)$ and $K_4Cu_4O_2(SO_4)_4 \cdot (Na,Cu)Cl$ crystallise in $I4$ space group, while $Na_4Cu_4O_2(SO_4)_4 \cdot (MCl)$ ($M = Na, Cu$ and \square) crystallises in $P4/n$. It can be seen that filling the channels with metal chloride ($MeCl$) complexes shows significant variations. It should be noted that the structural features of piypite from the fumaroles of Tolbachik volcano have not been studied to date. Effenberger and Zemann (1984) explicitly state in their article that “the nature of the Me atoms is not completely clear”.

$Rb_2Cu_2(SO_4)_3$ is a further example of crystallisation in the already known structure type first observed for $K_2Cu_2(SO_4)_3$ (Lander *et al.*, 2017). In $Rb_2Cu_2(SO_4)_3$, the unit-cell parameters increase significantly in accordance with an increase in the ionic radius of the alkali cation. The stoichiometry of the $A_2M_2^{2+}(SO_4)_3$ compounds corresponds to one of the most common potassium and magnesium sulfates – langbeinite, $K_2Mg_2(SO_4)_3$, which crystallises in the cubic space group $P2_13$. In the fumaroles of the scoria cones of the Tolbachik volcano, langbeinite is also one of the most common anhydrous sulfates. Langbeinite-type compounds show very wide variations in isomorphous substitutions (Gattow and Zemann, 1958). The main factor for the formation

of the $A_2Cu_2(SO_4)_3$ orthorhombic structure is the presence of Jahn–Teller copper cations. In the same series of syntheses, during which $Rb_2Cu_2(SO_4)_3$ was obtained, ‘hydrolangbeinite’ $Rb_2Cu_2(SO_4)_3(H_2O)$ was found, formed as a result of a minor hydration of the initial mixture of reagents. Hydrated langbeinites are currently unknown for any composition of minerals or synthetic compounds. The new compound obtained shows the probability of detecting such compounds (especially for copper-containing ones) in the zones of fumaroles exposed to intense atmospheric precipitation. Alkali copper sulfates are known to form multiple hydrated ‘offsprings’ during exposure to moist air (Siidra *et al.*, 2021a).

In the determined new structural architectures, a number of features were revealed which were seldom observed before. The first is the bidentate coordination of the sulfate tetrahedra via edge-sharing to the Cu^{2+} -centred coordination polyhedron. Until recently, such coordination was known only for the chlorothionite structure. The second is formation of ‘high-coordinated’ Cu atoms forming CuO_7 polyhedra. We considered such a coordination when describing the crystal structure of saranchinaite (Siidra *et al.*, 2018c). The structures of the new compounds suggest that such coordination is not in fact so uncommon, at least among anhydrous alkali copper sulfates. All of the described features clearly indicate the importance of further systematic studies of anhydrous copper-sulfate systems. Their exploration, particularly of the new copper-oxide substructures with new coordination environments, is highly likely to lead to new potentially interesting magnetic properties due to unusual arrangements of magnetically active Cu^{2+} cations. The effect of the alkali cation size on the Cu^{2+} coordination has been demonstrated recently for the family of synthetic hydrogen selenites (Charkin *et al.*, 2019); one can expect that it will also be pronounced in other families, including sulfates.

The crystallographic parameters listed in Tables 2–5, show that anhydrous sulfates are a fruitful playground for the synthesis of new anhydrous compounds known previously only as

Table 4. Crystallographic parameters of known chlorothionite-type $A_2Cu(SO_4)X_2$ compounds.

Phase type	α -type				β -type
	Synthetic	Chlorothionite	Synthetic	Synthetic	Synthetic
Mineral/synthetic					
Formula	$Na_2Cu(SO_4)Cl_2$	$K_2Cu(SO_4)Cl_2$	$K_2Cu(SO_4)Cl_2$	$K_2Cu(SO_4)Br_2$	$Rb_2Cu(SO_4)Cl_2$
Space group	<i>Pnma</i>	<i>Pnma</i>	<i>Pnma</i>	<i>Pnma</i>	<i>C2/c</i>
<i>a</i> (Å)	7.0324(2)	7.7320(15)	7.73	7.73	7.4645(7)
<i>b</i> (Å)	5.60540(10)	6.078(1)	6.08	6.30	16.0377(18)
<i>c</i> (Å)	16.0344(4)	16.2920(30)	16.29	16.43	7.6580(8)
β (°)					116.327(6)
<i>V</i> (Å ³)	632.07(3)	765.64	765.60	800.12	821.68(15)
<i>R</i> ₁	0.0244	0.032	–	–	0.019
Reference	Fujihala <i>et al.</i> (2020)	Giacovazzo <i>et al.</i> (1976)	Bo <i>et al.</i> (2020)	Bo <i>et al.</i> (2020)	this work

Table 5. Crystallographic parameters of known piypite-type $Rb_4[Cu_4O_2(SO_4)_4] \cdot (MCl)$ compounds.

Phase type	α -type	β -type	
	Synthetic	Piypite	Synthetic
Mineral/Synthetic			
Formula	$Na_4[Cu_4O_2(SO_4)_4] \cdot (MCl)$ (<i>M</i> = Na, Cu, □)	$K_4[Cu_4O_2(SO_4)_4] \cdot (MeCl)$	$Rb_4[Cu_4O_2(SO_4)_4] \cdot (Cu_{0.83}^{+}Rb_{0.17}^{-}Cl)$
Space group	<i>P4/n</i>	<i>I4</i>	<i>I4</i>
<i>a</i> (Å)	18.451(1)	13.60(2)	14.171(14)
<i>c</i> (Å)	4.9520(2)	4.98(1)	4.991(5)
<i>V</i> (Å ³)	1685.86(15)	921.1	1002(2)
<i>R</i> ₁	0.028	0.035	0.043
Reference	Kahlenberg <i>et al.</i> (2000)	Effenberg and Zemmann (1984)	this work

prototype-structures in minerals. Conversely, it is highly probable that compounds, obtained so far only as synthetics, may exist as minerals in high-temperature fumaroles with strongly oxidising conditions and in sublimates of natural coal fires (e.g. Pautov *et al.*, 2020).

It is worth noting here that synthetic analogues of various minerals, including sulfates, have been obtained using various synthetic approaches, which do not necessarily mimic the natural processes (or, more exactly, the currently assumed formation mechanisms). At present, condensation from a vapour phase or interaction of hot gases with basaltic scoria are considered to be the most likely formation mechanisms of fumarolic minerals. Yet, our studies clearly indicate that vapour transport in water-free systems can be ignored at least until 600°C wherein the only volatile species are copper chlorides. At least some of the compounds described herein have most probably crystallised from melts. Several test experiments have shown that at least some Rb-containing compositions melt at temperatures as low as 400–450°C; moreover, good-quality crystals and homogeneous samples were not produced even after long-time subsolidus heat treatments. Additional experiments are clearly necessary to elucidate the role of reaction kinetics in solid-state processes. The other synthetic approach, applied successfully to preparation of analogues of chlorothionite, is crystallisation from hot aqueous solutions. However, one can expect competitive formation of less soluble double sulfates, e.g. Tutton salts, or hydrolysis products, e.g. analogues of natrochalcite. Overall, the chemistry of hydrates with low water content remains in many respects a *terra incognita*. A possible solution lies in exploiting media with low chemical potential of water; our current example is the $Rb_2Cu_2(SO_4)_3(H_2O)$, formed under low vapour pressure (given the sealed tube had survived internal pressure upon annealing). A test experiment with the initially wet sulfate charge annealed in a temperature gradient between ambient and 650°C produced

good-quality single crystals of various known hydrates including $CuSO_4 \cdot 5H_2O$ in the relatively cold part of the sealed silica tube. Therefore, this approach is promising in producing various hydrates scarcely accessible in any other way. The use of moist non-aqueous solvents seems not to be straightforward as they either do not dissolve most inorganic sulfates (alcohols) or coordinate competitively to copper (acetonitrile). The process involving water evidently also takes place under natural conditions, e.g. upon hydration–dehydration cycles. Yet, our studies of such processes for selected copper sulfate minerals indicate that these are very complicated (Siidra *et al.*, 2021a), include numerous steps and are not always reversible even for initially single-phase specimens. It is however very likely that these studies, extended into more complex systems, will produce even more intricate and intriguing architectures, compositions and possibly properties. Some of these studies are now in progress.

Acknowledgements. We are grateful to Uwe Kolitsch, Gerald Giester and Peter Leverett for many valuable comments. Technical support by the SPbSU X-ray Diffraction Resource Centre is gratefully acknowledged.

Supplementary material. To view supplementary material for this article, please visit <https://doi.org/10.1180/mgm.2021.73>

References

- Bo X., Wang D., Wan B. and Wan X.G. (2020) Calculated magnetic exchange interactions in the quantum spin chain materials $K_2CuSO_4Cl_2$ and $K_2CuSO_4Br_2$. *Physical Reviews*, **B101**, 024416.
- Borisov A.S., Siidra O.I., Kovrugin V.M., Golov A.A., Depmeier W., Nazarchuk E.V. and Holzheid A. (2021) Expanding the family of mineral-like anhydrous alkali copper sulfate framework structures: New phases, topological analysis and evaluation of ion migration potentialities. *Journal of Applied Crystallography*, **54**, 237–250.
- Bruker (2014) APEX2. Version 2014.11-0. Bruker-AXS, Madison, Wisconsin, USA.

- Burns P.C. and Hawthorne, F.C. (1995) Coordination geometry pathways in Cu^{2+} oxysalt minerals. *The Canadian Mineralogist*, **33**, 889–905.
- Chaplygin I.V., Taran Y.A., Dubinina E.O., Shapar V.N. and Timofeeva I.F. (2015) Chemical composition and metal capacity of magmatic gases of Gorely volcano, Kamchatka. *Doklady Earth Sciences*, **463**, 690–694.
- Chaplygin I.V., Lavrushin V.Y., Dubinina E.O., Bychkova Y.V., Inguaggiato S. and Yudovskaya M.A. (2016) Geochemistry of volcanic gas at the 2012–13 New Tolbachik eruption, Kamchatka. *Journal of Volcanology and Geothermal Research*, **323**, 186–193.
- Charkin D.O., Markovski M.R., Siidra O.I., Nekrasova D.O. and Grishaev V.Yu. (2019) Influence of the alkali cation size on the Cu^{2+} coordination environments in $(\text{AX})[\text{Cu}(\text{HSeO}_3)_2]$ ($\text{A} = \text{Na}, \text{K}, \text{NH}_4, \text{Rb}, \text{Cs}$; $\text{X} = \text{Cl}, \text{Br}$) layered copper hydrogen selenite halides. *Zeitschrift für Kristallographie – Crystalline Materials*, **234**, 739–747.
- Churikova T., Dorendorf F. and Wörner G. (2001) Sources and fluids in the mantle wedge below Kamchatka, evidence from across-arc geochemical variation. *Journal of Petrology*, **42**, 1567–1593.
- Churikova T.G., Gordeychik B.N., Edwards B.R., Ponomareva V.V. and Zelenin E.A. (2015a) The Tolbachik volcanic massif: A review of the petrology, volcanology and eruption history prior to the 2012–2013 eruption. *Journal of Volcanology and Geothermal Research*, **307**, 3–21.
- Churikova T.G., Gordeychik B.N., Iwamori H., Nakamura H., Ishizuka O., Nishizawa T., Haraguchi S., Miyazaki T. and Vaglarov B.S. (2015b) Petrological and geochemical evolution of the Tolbachik volcanic massif, Kamchatka, Russia. *Journal of Volcanology and Geothermal Research*, **307**, 156–181.
- Effenberger H. and Zemann J. (1984) The crystal structure of caratiite. *Mineralogical Magazine*, **48**, 541–546.
- Fujihala M., Koorikawa H., Mitsuda S., Morita K., Tohyama T., Tomiyasu K., Koda A., Okabe H., Itoh S., Yokoo T., Ibuka S., Tadokoro M., Itoh M., Sagayama H., Kumai R. and Murakami Y. (2017) Possible Tomonaga-Luttinger spin liquid state in the spin-1/2 inequilateral diamond-chain compound $\text{K}_3\text{Cu}_3\text{AlO}_2(\text{SO}_4)_4$. *Scientific Reports*, **7**, 16785.
- Fujihala M., Sugimoto T., Tohyama T., Mitsuda S., Mole R.A., Yu D.H., Yano S., Inagaki Y., Morodomi H., Kawae T., Sagayama H., Kumai R., Murakami Y., Tomiyasu K., Matsuo A. and Kindo K. (2018) Cluster-based haldane state in an edge-shared tetrahedral spin-cluster chain: fedotovite $\text{K}_2\text{Cu}_3\text{O}(\text{SO}_4)_3$. *Physical Review Letters*, **120**, 077201.
- Fujihala M., Mitsuda S., Mole R.A., Yu D.H., Watanabe I., Yano S., Kuwai T., Sagayama H., Kouchi T., Kamebuchi H. and Tadokoro M. (2020) Spin dynamics and magnetic ordering in the quasi-one-dimensional $S=1/2$ antiferromagnet $\text{Na}_2\text{CuSO}_4\text{Cl}_2$. *Physical Reviews*, **B101**, 024410.
- Furrer A., Podlesnyak A., Pomjakushina E. and Pomjakushin V. (2018) Spin triplet ground-state in the copper hexamer compounds $\text{A}_2\text{Cu}_3\text{O}(\text{SO}_4)_3$ ($\text{A} = \text{Na}, \text{K}$). *Physical Reviews*, **B98**, 180410.
- Gattow G. and Zemann J. (1958) Über Doppelsulfatsalze vom Typ $\text{A}_2^+\text{B}_2^{2-}(\text{SO}_4)_3$. *Zeitschrift für Anorganische und Allgemeine Chemie*, **293**, 233–240.
- Giacovazzo C., Scandale E. and Scordari F. (1976) The crystal structure of chlorothionite $\text{CuK}_2\text{Cl}_2\text{SO}_4$. *Zeitschrift für Kristallographie – Crystalline Materials*, **144**, 226–237.
- Hawthorne F.C., Krivovichev S.V. and Burns P.C. (2000) The crystal chemistry of sulfate minerals. Pp. 1–112 in: *Sulfate Minerals – Crystallography, Geochemistry and Environmental Significance* (C.N. Alpers, J.L. Jambor and D.K. Nordstrom, editors). Reviews in Mineralogy and Geochemistry, **40**. Mineralogical Society of America and Geochemical Society, Washington D.C.
- Kahlenberg V., Piotrowski A. and Giester G. (2000) Crystal structure of $\text{Na}_4[\text{Cu}_4\text{O}_2(\text{SO}_4)_4]\cdot\text{MeCl}$ ($\text{Me} = \text{Na}, \text{Cu}, \square$) – the synthetic Na-analogue of pypite (caratiite). *Mineralogical Magazine*, **64**, 1099–1108.
- Korniyakov I.V., Vladimirova V.A., Siidra O.I. and Krivovichev S.V. (2021) Expanding the averievite family, $(\text{MX})\text{Cu}_5\text{O}_2(\text{T}^{5+}\text{O}_4)_2$ ($\text{T}^{5+} = \text{P}, \text{V}$; $\text{M} = \text{K}, \text{Rb}, \text{Cs}, \text{Cu}$; $\text{X} = \text{Cl}, \text{Br}$): synthesis and single-crystal X-ray diffraction study. *Molecules*, **26**, 833.
- Kovrugina V.M., Nekrasova D.O., Siidra O.I., Mentré O., Masquelier C., Stefanovich S.Yu. and Colmont M. (2019) Mineral-inspired crystal growth and physical properties of $\text{Na}_2\text{Cu}(\text{SO}_4)_2$, and review of $\text{Na}_2\text{M}(\text{SO}_4)_2(\text{H}_2\text{O})_x$ ($x = 0–6$) compounds. *Crystal Growth and Design*, **19**, 1233–1244.
- Lander L., Rouse G., Batuk D., Colin C.V., Dalla Corte D.A. and Tarascon J.-M. (2017) Synthesis, structure, and electrochemical properties of K-based sulfates $\text{K}_2\text{M}_2(\text{SO}_4)_3$ with $\text{M} = \text{Fe}$ and Cu . *Inorganic Chemistry*, **56**, 2013–2021.
- Marsh R.E. (1995) Some thoughts on choosing the correct space group. *Acta Crystallographica*, **B51**, 897–907.
- Masquelier C. and Croguennec L. (2013) Polyanionic (phosphates, silicates, sulfates) frameworks as electrode materials for rechargeable Li (or Na) batteries. *Chemical Reviews*, **113**, 6552–6591.
- Menyailov I.A. and Nikitina L.P. (1980) Chemistry and metal contents of magmatic gases: the new Tolbachik volcanoes case (Kamchatka). *Bulletin Volcanologique*, **43**, 195–205.
- Nekrasova D.O., Tsirlin A.A., Colmont M., Siidra O.I., Vezin H. and Mentré O. (2020) Magnetic hexamers interacting in layers in the $(\text{Na},\text{K})_2\text{Cu}_3\text{O}(\text{SO}_4)_3$ minerals. *Physical Reviews*, **B102**, 184405.
- Nekrasova D.O., Siidra O.I., Zaitsev A.N., Ugolkov V.L., Colmont M., Charkin D.O., Mentré O., Chen R., Kovrugina V.M. and Borisov A.S. (2021) A fumarole in a one-pot: synthesis, crystal structure and properties of Zn- and Mg-analogues of itelmenite and a synthetic analogue of glikinite. *Physics and Chemistry of Minerals*, **46**, 6.
- Pautov L.A., Mirakov M.A., Siidra O.I., Faiziev A.R., Nazarchuk E.V., Karpenko V.Yu. and Makhmadsharif S. (2020) Falgarite, $\text{K}_4(\text{VO})_3(\text{SO}_4)_5$, a new mineral from sublimates of a natural underground coal fire at the tract of Kukhi-Malik, Fan-Yagnob coal deposit, Tajikistan. *Mineralogical Magazine*, **84**, 455–462.
- Pekov I.V., Zubkova N.V., Yapaskurt V.O., Belakovskiy D.I., Chukanov N.V., Lykova I.S., Savelyev D.P., Sidorov E.G. and Pushcharovskiy D.Yu. (2014) Wulffite, $\text{K}_3\text{NaCu}_4\text{O}_2(\text{SO}_4)_4$, and parawulffite, $\text{K}_5\text{Na}_3\text{Cu}_8\text{O}_4(\text{SO}_4)_8$, two new minerals from fumarole sublimates of the Tolbachik volcano, Kamchatka, Russia. *The Canadian Mineralogist*, **52**, 699–716.
- Pekov I.V., Zubkova N.V. and Pushcharovskiy D.Y. (2018a) Copper minerals from volcanic exhalations – a unique family of natural compounds: crystal-chemical review. *Acta Crystallographica*, **B74**, 502–518.
- Pekov I.V., Zubkova N.V., Agakhanov A.A., Pushcharovskiy D.Yu., Yapaskurt V.O., Belakovskiy D.I., Vigasina M.F., Sidorov E.G. and Britvin S.N. (2018b) Cryptochalcite, $\text{K}_2\text{Cu}_5\text{O}(\text{SO}_4)_5$, and cesiodymite, $\text{CsKC}_5\text{O}(\text{SO}_4)_5$, two new isotypic minerals and the K-Cs isomorphism in this solid-solution series. *European Journal of Mineralogy*, **30**, 593–607.
- Popolitov E.I. and Volynets O.N. (1982) Geochemistry of quaternary volcanic rocks from the Kurile-Kamchatka island arc. *Journal of Volcanology and Geothermal Research*, **12**, 299–316.
- Portnyagin M., Duggen S., Hauff F., Mironov N., Bindeman I., Thirlwall M. and Hoernle K. (2015) Geochemistry of the late Holocene rocks from the Tolbachik volcanic field, Kamchatka: Quantitative modelling of subduction-related open magmatic systems. *Journal of Volcanology and Geothermal Research*, **307**, 133–155.
- Rouse G. and Tarascon J.-M. (2014) Sulfate-based polyanionic compounds for Li-ion batteries: synthesis, crystal chemistry, and electrochemistry aspects. *Chemistry of Materials*, **26**, 394–406.
- Scordari F. and Stasi F. (1990) The crystal structure of euchlorine, $\text{NaKC}_5\text{O}(\text{SO}_4)_5$, Locality: Vesuvius, Italy. *Neues Jahrbuch für Mineralogie Abhandlungen*, **161**, 241–253.
- Sheldrick G.M. (2015) Crystal structure refinement with SHELXL. *Acta Crystallographica*, **B71**, 3–8.
- Siidra O.I., Nazarchuk E.V., Zaitsev A.N., Lukina E.A., Avdontseva E.Y., Vergasova L.P., Vlasenko N.S., Filatov S.K., Turner R. and Karpov G.A. (2017) Copper oxosulphates from fumaroles of Tolbachik Volcano: puninite, $\text{Na}_2\text{Cu}_3\text{O}(\text{SO}_4)_3$ – a new mineral species and structure refinements of kamchatkite and alumoklyuchevskite. *European Journal of Mineralogy*, **29**, 499–510.
- Siidra O.I., Nazarchuk E.V., Lukina E.A., Zaitsev A.N. and Shilovskikh V.V. (2018a) Belousovite, $\text{KZn}(\text{SO}_4)\text{Cl}$, a new sulphate mineral from the Tolbachik volcano with apophyllite sheet-topology. *Mineralogical Magazine*, **82**, 1079–1088.
- Siidra O.I., Kozin M.S., Depmeier W., Kayukov R.A. and Kovrugina V.M. (2018b) Copper – lead selenite bromides: A new large family of compounds partly having Cu^{2+} substructures derivable from Kagome-nets. *Acta Crystallographica*, **B74**, 712–724.
- Siidra O.I., Lukina E.A., Nazarchuk E.V., Depmeier W., Bubnova R.S., Agakhanov A.A., Avdontseva E.Yu., Filatov S.K. and Kovrugina V.M. (2018c)

- Saranchinaite, $\text{Na}_2\text{Cu}(\text{SO}_4)_2$, a new exhalative mineral from Tolbachik Volcano, Kamchatka, Russia, and a product of the reversible dehydration of kröhnkite, $\text{Na}_2\text{Cu}(\text{SO}_4)_2(\text{H}_2\text{O})_2$. *Mineralogical Magazine*, **82**, 257–274.
- Siidra O.I., Borisov A.S., Lukina E.A., Depmeier W., Platonova N.V., Colmont M. and Nekrasova D.O. (2019a) Reversible hydration/dehydration and thermal expansion of euchlorine, ideally $\text{KNaCu}_3\text{O}(\text{SO}_4)_3$. *Physics and Chemistry of Minerals*, **46**, 403–416.
- Siidra O.I., Nazarchuk E.V., Agakhanov A.A. and Polekhovskiy Yu.S. (2019b) Aleutite $[\text{Cu}_5\text{O}_2](\text{AsO}_4)(\text{VO}_4) \cdot (\text{Cu}_{0.5}\square_{0.5})\text{Cl}$, a new complex salt-inclusion mineral with Cu^{2+} substructure derived from Kagome-net. *Mineralogical Magazine*, **83**, 847–853.
- Siidra O.I., Nazarchuk E.V., Zaitsev A.N. and Shilovskikh V.V. (2020) Majzlanite, $\text{K}_2\text{Na}(\text{ZnNa})\text{Ca}(\text{SO}_4)_4$, a new anhydrous sulphate mineral with complex cation substitutions from Tolbachik volcano. *Mineralogical Magazine*, **84**, 153–158.
- Siidra O.I., Borisov A.S., Charkin D.O., Depmeier W. and Platonova N.V. (2021a) Evolution of fumarolic anhydrous copper sulfate minerals during successive hydration/dehydration. *Mineralogical Magazine*, **85**, 262–277.
- Siidra O.I., Charkin D.O., Kovrugin V.M. and Borisov A.S. (2021b) $\text{K}(\text{Na},\text{K})\text{Na}_2[\text{Cu}_2(\text{SO}_4)_4]$: a new highly porous anhydrous sulfate and evaluation of possible ion migration pathways. *Acta Crystallographica B*. in press.
- Soldatov T.A., Smirnov A.I., Povarov K.Yu., Hälg M., Lorenz W.E.A. and Zheludev A. (2018) Spin gap in the quasi-one-dimensional $\text{S}=\frac{1}{2}$ antiferromagnet $\text{K}_2\text{CuSO}_4\text{Cl}_2$. *Physical Reviews*, **B98**, 144440.
- Symonds R.B. and Reed M.H. (1993) Calculation of multicomponent chemical equilibria in gas-solid liquid systems: calculation methods, thermochemical data, and applications to studies of high-temperature volcanic gases with examples from Mount St. Helens. *American Journal of Science*, **293**, 758–864.
- Taran Yu.A., Hedenquist J.W., Korzhinsky M.A., Tkachenko S.I. and Shmulovich K.I. (1995) Geochemistry of magmatic gases from Kudryavy volcano, Iturup, Kuril Islands. *Geochimica et Cosmochimica Acta*, **59**, 1749–1761.
- Tedesco D. and Toutain J.-P. (1991) Chemistry and emission rate of volatiles from White Island Volcano (New Zealand). *Geophysical Research Letters*, **18**, 113–116.
- Vergasova L.P. and Filatov S.K. (2012) New mineral species in products of fumarole activity of the Great Tolbachik Fissure Eruption. *Journal of Volcanology and Seismology*, **6**, 281–289.
- Vergasova L.P., Filatov S.K., Serafimova E.K. and Stalova G.L. (1984) Piypite $\text{K}_2\text{Cu}_2\text{O}(\text{SO}_4)_2$ - a new mineral of volcanic sublimates. *Doklady USSR Academy of Sciences, Earth Science Sections*, **275**, 714–717.
- Vergasova L.P., Starova G.L., Filatov S.K. and Anan'ev V.V. (1998) Averievite $\text{Cu}_5(\text{VO}_4)_2\text{O}_2 \cdot n\text{MX}$ - a new mineral of volcanic exhalations. *Doklady Akademii Nauk*, **359**, 804–807.
- Volynets A.O., Edwards B.R., Melnikov D., Yakushev A. and Griboedova I. (2015) Monitoring of the volcanic rock compositions during the 2012–2013 fissure eruption at Tolbachik volcano, Kamchatka. *Journal of Volcanology and Geothermal Research*, **307**, 120–132.
- Zelenski M.E., Fischer T.P., de Moor J.M., Marty B., Zimmermann L., Ayalew D., Nekrasov A.N. and Karandashev V.K. (2013) Trace elements in the gas emissions from the Erta Ale volcano, Afar, Ethiopia. *Chemical Geology*, **357**, 95–116.
- Zelenski M., Malik N. and Taran Y. (2014) Emissions of trace elements during the 2012–2013 effusive eruption of Tolbachik volcano, Kamchatka: Enrichment factors, partition coefficients and aerosol contribution. *Journal of Volcanology and Geothermal Research*, **285**, 136–149.
- Zelenski M., Kamenetsky V.S. and Hedenquist J. (2016) Gold recycling and enrichment beneath volcanoes: A case study of Tolbachik, Kamchatka. *Earth and Planetary Science Letters*, **437**, 35–46.
- Zhou H.A., Liu Z., Ang S.S. and Zhang J.-J. (2020) Synthesis, structure, and electrochemical performances of a novel three-dimensional framework $\text{K}_2[\text{Cu}(\text{SO}_4)_2]$. *Solid State Sciences*, **100**, 106104.